Accepted Manuscript

Discovery of 2-oxo-1,2-dihydrobenzo[cd]indole-6-sulfonamide derivatives as new RORγ inhibitors using virtual screening, synthesis and biological evaluation

Zhang Yan, Xue Xiaoqian, Jin Xiangyu, Song Yu, Li Jing, Luo Xiaoyu, Song Ming, Yan Weiqun, Song Hongrui, Xu Yong, PhD

PII: S0223-5234(14)00279-7

DOI: 10.1016/j.ejmech.2014.03.065

Reference: EJMECH 6849

To appear in: *European Journal of Medicinal Chemistry*

Received Date: 13 February 2014

Revised Date: 19 March 2014

Accepted Date: 22 March 2014

Please cite this article as: Z. Yan, X. Xiaoqian, J. Xiangyu, S. Yu , L. Jing, L. Xiaoyu, S. Ming, Y. Weiqun, S. Hongrui, X. Yong, Discovery of 2-oxo-1,2-dihydrobenzo[cd]indole-6-sulfonamide derivatives as new RORγ inhibitors using virtual screening, synthesis and biological evaluation, *European Journal of Medicinal Chemistry* (2014), doi: 10.1016/j.ejmech.2014.03.065.

Benzo[cd]indol-2(1H)-one derivatives were developed as new RORγ inhibitors for developing therapeutic drug treating Th17 mediated autoimmune diseases.

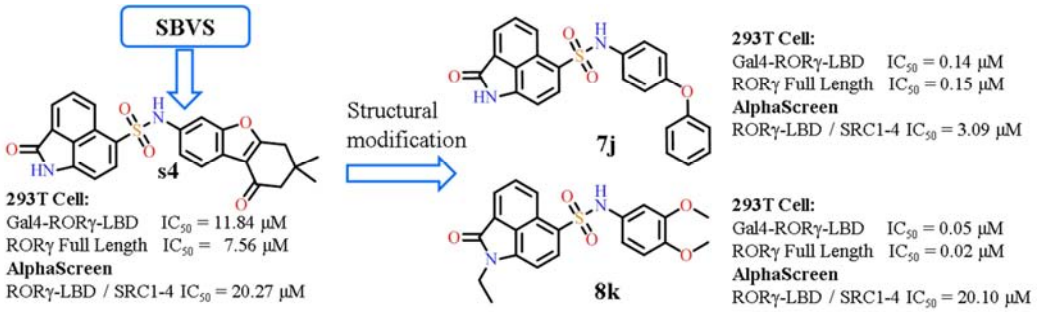

- RORγ is a promising drug target for treating Th17-mediated autoimmune diseases.
- A hit compound was obtained by structure-based virtual screening.
- 77 new compounds were designed and prepared starting from the hit compound.
- Several compounds acted as RORγ inhibitors and exhibited promising activities.
- SARs were analyzed based on predicted binding modes and assessed activity.

Discovery of 2-oxo-1,2-dihydrobenzo[cd]indole-6-sulfonamide derivatives as new RORγ inhibitors using virtual screening, synthesis and biological evaluation

Zhang Yan[a,1], Xue Xiaoqian[a,b,1], Jin Xiangyu[a,c], Song Yu [a,c], Li Jing[a], Luo Xiaoyu[a], Song Ming[a], Yan Weiqun[c], Song Hongrui[b], Xu Yong[a,*]

[a]Institute of Chemical Biology, Guangzhou Institutes of Biomedicine and Health, Chinese Academy of Sciences, No.190 Kaiyuan Avenue, Guangzhou Science Park, Guangzhou, Guangdong 510530, China

[b]School of Pharmaceutical Engineering, Shenyang Pharmaceutical University, No.103 Wenhua Road, Shenhe District, Shenyang, Liaoning 110016, China

[c]Department of Bioengineering School of Pharmaceutical Sciences, Jilin University, No.1266 Fujin Road, Chaoyang District, Changchun, Jilin 130021, China

[*]Corresponding Author: Yong Xu, PhD; E-mail: xu_yong@gibh.ac.cn

[1]These authors contributed equally to this work.

Key words:

RORγ inhibitor, Th17 cell differentiation, virtual screening, nuclear hormone receptor.

Abbreviations:

RORγ, Retinoic acid-related orphan receptor γ; LBD, ligand binding domain; LBP, ligand binding pocket; IC_{50}, 50% inhibitory concentration; SAR, structure activity relationship; AlphaScreen, Amplified Luminescence Proximity Homogeneous Assay

Abstract:

Retinoic acid-related orphan receptor γ (RORγ), a member of the nuclear hormone receptor superfamily, is a promising therapeutic target for treating Th17-mediated autoimmune diseases. We performed structure-based virtual screening targeting the RORγ ligand-binding domain. Among the tested compounds, **s4** demonstrated RORγ antagonistic activities with micromolar IC_{50} values in both an AlphaScreen assay (20.27 μM) and a cell-based reporter gene assay (11.84 μM). Optimization of the **s4** compound led to the identification of compounds **7j**, **8c**, **8k**, and **8p**, all of which displayed significantly enhanced RORγ inhibition with IC_{50} values of 40-140 nM. These results represent a promising starting point for developing potent small molecule RORγ inhibitors.

1. Introduction

T-helper 17 (Th17) cells are crucial effector cells that have been implicated in the pathology of a variety of human inflammatory and autoimmune diseases, including multiple sclerosis, rheumatoid arthritis, psoriasis, and inflammatory bowel disease [1]. In Th17 cells, interleukin-17 (IL-17) transcription is mediated by Th17-specific transcriptional regulators retinoic acid receptor-related orphan receptor α and γ (RORα and RORγ) [2,3]. In the experimental autoimmune encephalomyelitis (EAE) mouse model, suppression of IL-17 activity reduced severity of the inflammation symptom. Inhibition of RORγ may lead to enhanced anti-inflammatory activity. RORγ is ligand-dependent transcriptional factor that belongs to the nuclear hormone receptor superfamily. A large number of drugs have been developed to target nuclear receptor superfamily members. Given its crucial role in suppression of IL-17 activity, RORγ is a promising therapeutic target for treating Th17-mediated autoimmune diseases [4].

Since the identification of benzenesulfonamide liver X receptor (LXR) agonist T0901317 as an inverse RORγ agonist [5], several small molecule RORγ ligands have been disclosed in the literature (**Figure 1**) [6,7]. Digoxin and its less toxic analogues selectively antagonize RORγ and suppress Th17 cell differentiation [8,9]. Ursolic acid, a natural carboxylic acid that is ubiquitously present in plants, also suppressed IL-17 production by selectively inhibiting RORγ [10]. However, digoxin is a cardiac glycoside used for treating various heart conditions with a narrow therapeutic index, and ursolic acid also activates the glucocorticoid receptor, another nuclear receptor. Thus, the utility of those two natural products as candidates for further development is limiting. Using the T0901317 scaffold as a lead compound, Griffin el al. developed a series of synthetic RORγ antagonists, including SR1001, SR2211, and SR1555 [11-13]. Littman et al. identified diphenylpropanamide derivatives (**Figure 1**, ML209) as RORγ antagonists via quantitative high-throughput screening using a cell-based RORγ gene reporter assay [14]. Although significant progress has been made in

developing RORγ antagonists [15-17], the identification of novel, non-steroidal RORγ antagonists for therapeutic use still remains an urgent need.

In this study, we report the successful application of structure-based virtual screening in novel RORγ antagonist discovery. We screened a commercial small molecule database with approximately 220,000 compounds that was provided by Specs Ltd. Several non-steroidal compounds were identified as RORγ antagonists in a biological assay. Of these, the **s4** hit compound bearing a 2-oxo-1,2-dihydrobenzo[cd]indole-6-sulfonamide scaffold was selected as a starting point for further structural optimization. In total, 77 derivatives were designed, synthesized or purchased, and these were assessed in a bioassay. Several derivatives had better suppression of the RORγ basal transcriptional activity than the starting compound **s4**. The most potent compounds **7j**, **8c**, **8k**, and **8p** inhibited RORγ with IC_{50} values of 40-140 nM. Their RORγ antagonism was 300-fold higher than the hit compound **s4**. These compounds thus represent a promising starting point for developing potent small molecule RORγ antagonist with the potential for treatment of autoimmune diseases.

2. Results and discussion

2.1. Virtual screening

Structure-based virtual screening (SBVS) has been widely used in drug discovery. There are several successful examples of SBVS, particularly in nuclear receptor ligand discovery [18-20]. A schematic representation of the hit discovery strategy used in this work is presented in **Figure 2**. In this study, SBVS was first performed with the molecular docking program Glide, implemented in Schrödinger. After hierarchical molecular docking, post-processing and expert inspection, 24 compounds were selected based on their docking score, docking pose, hydrogen bond and hydrophobic interaction characterizations. Candidates were purchased from Specs Ltd. for further biological assay.

All of the selected compounds were assessed for their inhibitory activity using the AlphaScreen biochemical assay, which is a widely used assay for assessing ligand-dependent interactions between nuclear receptors and their co-regulators [21-23]. In the present study, we monitored RORγ ligand binding domain (LBD) interactions with the fourth LXXLL motif of coactivator SRC1 (SRC1-4) in the presence of the assessed compounds. Among the 24 molecules (**Supplementary Figure S1, Table S1**), 13 compounds demonstrated over 50% inhibition at 50 μM concentration in the AlphaScreen assay (**Supplementary Figure S2**). Compound **s4** was characterized by a completely new scaffold (**Figure 1**), and it demonstrated moderate antagonistic activity in the AlphaScreen assay (IC_{50} = 20.27 μM) and a cell-based luciferase reporter gene assay (IC_{50} = 11.84 μM) (**Supplementary Table S2)**. To investigate the receptor-ligand interaction details, the binding mode was predicted by molecular docking, as demonstrated in **Figure 3**. In compound **s4**, the carbonyl oxygen on the amide group forms a strong hydrogen bond with Arg367 of helix H5, and the NH of the sulfonamide group forms a direct hydrogen bond with Phe377. A π-π interaction exists between the ligand and the phenyl group in region B (**Figure 1**). These structure and interaction characterizations are common for nuclear receptor ligands. The compound anchors to the hydrophobic LBD through some conserved hydrogen bonds. **s4** was therefore selected as the starting point for further structural optimization.

2.2. Chemistry

Compound **s4** (**Figure 1**) features a 2-oxo-1,2-dihydrobenzo[cd]indole-6-sulfonamide scaffold and was selected as a template for new RORγ antagonist optimization. Considering the predicted interactions between **s4** and the residues in the RORγ LBD, we kept the common benzo[cd]indol-2(1H)-one moiety and modified two regions of this molecule to improve antagonistic activity (**Figure 1**). First, the hydrogen atom in region A was replaced with an ethyl to explore whether a larger group was tolerable. The amine group in region B was then replaced with different primary and secondary amines to explore how shape, hydrophobicity, and flexibility affect potency.

A general procedure for the synthesis of the designed compounds (**6**, **7**, **8**) is outlined in **Scheme 1**. The commercially available benzo[de]isochromene-1,3-dione (**1**) reacted with PTSA in the presence of pyridine to produce compound **2**, which was then reacted with NaOH followed by HCl treatment to produce compound **3**. Subsequently, compound **3** was reacted with ethyl iodide in DMF to produce compound **4**, and compound **4** was then reacted with chlorosulfonic acid in chloroform to obtain compound **5**. Finally, the target compounds (**6**, 7, 8) were obtained from the reactions of compound **5** with different amines.

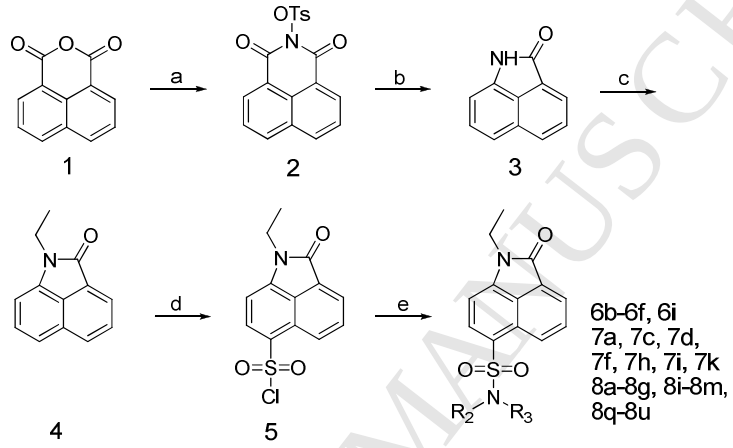

Scheme 1. Synthesis of 2-oxo-1,2-dihydrobenzo[cd]indole-6-sulfonamide derivatives.

Reagents and conditions: (a) $NH_4OH{\cdot}HCl$, pyridine, PTSA, 95 ˚C, 1 h; (b) (1) 2.7 mol/L NaOH, EtOH, H_2O, reflux, 3 h; (2) HCl, rt 30 min; (c) NaH, C_2H_5I, DMF, 0 ˚C to rt 3 h; (d) HSO_3Cl, $CHCl_3$, 0 ˚C to 50 ˚C, 6.0 h; (e) R_2-NH-R_3, DMAP, TEA, DMF, rt overnight or DIPEA, DCM, rt overnight or 2,6-lutidine, THF/acetone=1:1, 65 ˚C, overnight or pyridine, rt overnight.

2.3. SAR study

Starting from the hit compound **s4**, we purchased and synthesized 77 compounds. First, we investigated the influence of different fused heterocyclic ring derivatives in a protein-based AlphaScreen assay and a cell-based reporter gene assay. For the cell-based reporter gene assay, we determined the RORγ transcriptional activity using a widely used Gal4-driven promoter. We also assessed compounds for their suppression of the transcriptional activity of the RORγ reporter gene that contained the natural ROR response element (RORE), which was derived from the Purkinje cell protein 2 gene (see **experimental section** for details) [23]. Dose response curves for T0901317 and compounds in this study are demonstrated in **Supplementary Figure**

S4. For most compounds, the suppression effects of the basal transcriptional activity for both RORγ LBD and full length RORγ are similar. As demonstrated in **Table 1**, compound **6a** demonstrated 11-fold improved inhibition compared with **s4** in a reporter gene assay, while adding one flexible carbon atom between the scaffold and the fused heterocyclic ring completely abolished inhibition (**6b**, **6c**, **6d**, **6e** vs. **6a**). Compound **6f** contained an isoquinoline group on the right side and demonstrated significant improvement with an IC_{50} value of 0.10 μM. Naphthalene (**6g**), benzofuran (**6h**), or indoline (**6i**) derivatives resulted in complete loss of RORγ inhibition.

To further explore SAR, substituents with different rings that were linked by linkers of various lengths were attached to sulfonamide (**Table 2**). Introduction of a 4-morpholinophenyl moiety increased RORγ potency by more than 35-fold (**7a** vs. **s4**). An ethyl substituent at the R_1 position did not greatly alter the potency (**7b** vs. **7a**), while increasing linker flexibility by adding 3 carbon atoms to the morpholine group resulted in a loss of inhibition (**7d** vs. **7a**). Modifying the substituent R_3 from 4-morpholinophenyl (**7a**) to biphenyl-4-yl (**7e**) also resulted in a loss of inhibition. Introducing of a 3-morpholinophenyl (**7f**) to the R_3 position completely abolished inhibition, suggesting that the substituent position and hydrophobic properties are critical for binding (**7f** vs. **7a**). Similar to **7f**, compounds **7g**, **7h** and **7i** did not demonstrate any inhibition. Interestingly, inserting an oxygen atom between biphenyl groups dramatically improved RORγ inhibition and had an IC_{50} of 0.14 μM (**7j** vs. **7e**). The compounds with relatively rigid diazene (**7k**) or amide (**7m**) linkers demonstrated moderate gains in cellular activity.

To investigate the spatial effect, smaller compounds were also obtained and assessed for SAR analysis (**Table 3**). There was a slight increase in inhibition with the introduction of a *tert*-butyl carbamate group at the *meta*-position of the phenyl group (**8a** vs. **s4**), which was completely lost with a similar group attached to piperidine ring at the R_3 position (**8b**). An acetyl group attached to both the phenyl and piperidine groups resulted in significant gains in cellular activity; however, an aromatic phenyl

group was preferred. Compound **8f**, which has an acetyl group at the *ortho*-position of the phenyl group, was inactive, while **8g** and **8c** have an acetyl group at the *meta*- or *para*-position and were ranked as the most potent RORγ antagonists. Modifying the substituent from 3-*tert*-butyl phenyl (**8i**) to 2-tert-butyl phenyl (**8j**) caused a loss of inhibition. Compound **8k**, which bears a 3,4-dimethoxybenzyl group, demonstrated comparable activity to **8c** and **8g**. Adding another substituent group at the R_2 position resulted in similar inhibition (**8p** vs. **8k**). Adding one atom before the aromatic ring resulted in a loss of inhibition (**8m**, **8r**, **8t**, **8u**), but adding small substituents, such as a halogen atom, caused minor gains in activity (**8s**, **8q** and others not listed in this table), which is presumably because of the disruption of the π-π stacking interaction between the ligand and LBD residues.

To rationalize the SAR between these novel inhibitors and RORγ, we investigated ligand binding modes within the LBD using a molecular docking method. The crystal structure demonstrated that digoxin bound in the ligand-binding pocket of RORγ [9]. Three O atoms of digoxin made direct hydrogen bonds with Phe377 in β-strand 1, Arg367 in helix H5 and His479 in helix H11. Two O atoms of digoxin formed hydrogen bonds via water molecules with Glu379 in loop s1-s2 and Val367 in the H5. A recently reported crystal structure demonstrated that T0901317 (PDB code 4NB6.pdb) is bound in the RORγ ligand-binding pocket. In the ligand binding pocket, the phenyl-sulfonamide group on T0901317 forms a unique π-π stacking interaction with Phe378, Phe388 and Phe401 [15]. In the present study, compound **s4** directly forms two hydrogen bonds with residues in the LBD. The carbonyl oxygen on the amide forms a strong hydrogen bond with Arg367 of H5, while the NH of the sulfonamide group makes a direct hydrogen bond with the carboxyl oxygen atom of the Phe377 backbone. Strong π-π interactions also exist between the inhibitors and Phe378, Phe388 and Phe401. All of the compounds presented here bear similar structural characteristics but differ in shape and flexibility on the right side. The predicted binding modes of the most potent compounds, **7j, 8c, 8k, 8p**, are demonstrated in **Figure 4** (see **Supplementary Figure S3** for other compounds). The

2-oxo-1,2-dihydrobenzo[cd]indole-6-sulfonamide moiety on the left side fits snugly into the hydrophobic pocket, and the polar head forms a conserved hydrogen bond with Arg367. This bulky group linked with a sulfonamide restrains the direction of the R_3 group. The phenyl group close to the sulfonamide NH forms a strong π-π interaction; however, the rigid substituent group connected to this phenyl group reduces potency because of steric conflicts with Ile397 (**7e**, **7f**, **7g**). This phenyl group is important for potency because of the strong π-π interaction, and two aromatic rings linked with a flexible atom are able to maintain the potency of the compounds (**7k**, **7m**, **7j**). The compounds bearing a flexible linker with different carbon chain lengths or piperidine rings lose inhibition in both the reporter gene assay and the protein-based AlphaScreen assay (**7c**, **7d**, **8e**, **8m**, **8q**, **8r**, **8t**, **8u** and **7h**, **8b**). The most potent and simple substitute is a small aromatic phenyl ring (**8g**, **8k**, **8p**). Further medicinal chemistry optimization should be performed with small or flexible substituents on the right side or a small substituent on the left side.

3. Conclusion

In summary, we have discovered a new series of RORγ antagonists using a structure-based virtual screening approach in conjunction with medicinal chemistry optimization and biological evaluation. Based on the initial hit compound **s4**, 77 derivatives were synthesized or purchased and assessed with the AlphaScreen assay and the luciferase reporter gene assays. Of these, 20 derivatives demonstrated remarkably improved activity; the most potent compounds, **7j, 8c, 8k, 8p**, demonstrated 300-fold improvement compared with compound **s4**. SAR analysis demonstrated that changes in R_3 group substituents critically influenced antagonistic activity. Further left side structural optimization and in vivo studies are currently in progress and will be reported in due course.

4. Experimental section

4.1. Molecular docking

The crystal structure of RORγ in complex with the antagonist digoxin (PDB code:

3B0W.pdb) was used as the reference structure in the docking study. Protein structure preparation for docking studies included water deletion, hydrogen atom addition and protonation state adjustment. All of the ligand and protein preparation were performed in Maestro (version 9.4, Schrödinger, LLC, New York, NY, 2013) implemented in the Schrödinger program (http://www.schrödinger.com). The Specs database subset with nearly 220,000 compounds was selected and downloaded from the ZINC website (http://zinc.docking.org) for virtual screening. In this study, structure-based virtual screening was performed with the Glide molecular docking program (version 6.1, Schrödinger, LLC, New York, NY, 2013) using the high-throughput virtual screening (HTVS), Glide SP, and Glide XP modes. For all of the methods, glide docks flexible ligands into a rigid receptor structure. Final ranking from the docking was based on the docking score, which combines the Epik state penalty with the Glide Score. Glide HTVS docking without using any constraints output the top 20,000 structures for next step evaluation. Using hydrogen bond constraints with Arg367, Glide SP output 5000 structures based on the docking score. These 5000 structures were further evaluated with Glide XP, and 115 compounds were kept according to their binding mode and docking scores (lower than -9.0 kcal/mol). Finally, 24 compounds were selected and purchased from Specs Ltd. for subsequent biological evaluation (**Supplementary Figure S1** and **Table S1**). For these compounds, which were obtained from the substructure search or were optimized from **s4**, molecular docking was performed to predict the plausible binding mode and binding affinity.

4.2. Substructure and similarity search

To obtain structurally similar compounds to **s4** from the Specs database, a substructure search or similarity search was performed using the Canvas module as implemented in Schrödinger. Part of **s4** was used as a query structure, and 292 compounds were obtained; the resulting structures were clustered according to their functional-class fingerprints using the hierarchical cluster protocol in Canvas. Of these, 37 compounds were selected based on their Fpscreen score and structural diversity, and they were then purchased from Specs Ltd.

4.3. Chemistry

The reagents were purchased from commercial sources and used without further

purification. For the synthesized compounds described below, flash chromatography was performed using silica gel (300-400 mesh). All of the reactions were monitored by TLC using silica gel plates (fluorescence F254, UV light). ^{1}H-NMR spectra were recorded on a Bruker AV-400 spectrometer at 400 MHz. Coupling constants (*J*) were expressed in hertz (Hz). ^{13}C-NMR spectra were recorded at 400 or 500 MHz. Chemical shifts (δ) were reported in parts per million (ppm) (using TMS as an internal control). Signals were described as singlet (s), doublet (d), triplet (t), quartet (q), multiplet (m), and broad (br). The low- or high-resolution mass spectra (LRMS and HRMS) were measured on an Agilent 1200 HPLC-MSD mass spectrometer or an Applied Biosystems Q-STAR Elite ESI-LC-MS/MS mass spectrometer, respectively. (See **Supplementary Figure S5** for ^{1}H-NMR and ^{13}C-NMR spectra of compounds **6f**, **7a**, **7k**, **8a**, **8c**, **8i**, **8k** and **8s**).

*4.3.1. 1,3-dioxo-2,3-dihydro-1H-phenalen-2-yl 4-methylbenzenesulfonate (**2**).*

To a solution of compound **1** (11.9 g, 60 mmol) in pyridine (70 mL) was added hydroxylamine hydrochloride (4.18 g, 60 mmol). The reaction mixture was heated to reflex temperature for 1 h followed by cooling to 80 ˚C. Powdered p-toluenesulfonyl chloride (22.9 g, 120 mmol) was added to the system mixture refluxed for 1 h. After cooling to room temperature, the reaction mixture was poured into ice water (1000 mL) and stirred to precipitate crystals. The precipitate was filtered and rinsed with additional cool water (100 mL) and saturated $NaHCO_3$ (100 mL) to give the title compound (17.2 g, 78% yield). The compound was used for the next step without further purification. MS (ESI), m/z for $C_{20}H_{14}O_5S$ ($[M + H]^+$): Calcd 366.06, found 367.0.

*4.3.2. Benzo[cd]indol-2(1H)-one (**3**).*

To a solution of compound **2** (17.2 g, 47 mmol) in ethanol (50 mL) and water (40 mL) was added an aqueous solution of sodium hydroxide (2.7 mol/L, 60 mL) at room temperature. The mixture was heated to reflux temperature for 3 h while distilling the ethanol. After the reaction was completed, the reaction mixture was cooled to 75 ˚C, concentrated hydrochloric acid was added dropwise, and a yellow precipitate was

formed. Then, the mixture was further cooled. The precipitate was collected by filtration and washed with water (100 mL×2). The resulting crude product was purified by silica gel chromatography with dichloromethane to give the title product as a yellow solid (6.65 g, 82%). MS (ESI), m/z for $C_{11}H_7NO$ ($[M + H]^+$): Calcd 169.05, found 170.0.

*4.3.3. 1-ethylbenzo[cd]indol-2(1H)-one (**4**).*

Compound **3** (6.65 g, 39 mmol) and sodium hydride (2.81 g, 117 mmol) were dissolved in DMF (100 mL) and cooled to 0 ˚C. Ethyl iodide (7.33 g, 47 mmol) was added dropwise. The reaction mixture was stirred at 0 ˚C for approximately 0.5 h. The cooling bath was removed, and the reaction mixture was stirred at room temperature. TLC demonstrated that the reaction was complete, and ice water (200 mL) was added. The reaction mixture was extracted with ethyl acetate (150 mL×2). The organic layer was washed with brine and dried over Na_2SO_4. The solid was filtered off, and the filtrate was concentrated under reduced pressure. The resulting crude product was purified by silica gel chromatography with petroleum ether/ethyl acetate (10/1, v/v) to yield the title product as a yellow oil (6.46 g, 84%). MS (ESI), m/z for $C_{11}H_{11}NO$ ($[M + H]^+$): Calcd 197.08, found 198.0.

*4.3.4. 1-ethyl-2-oxo-1,2-dihydrobenzo[cd]indole-6-sulfonyl chloride (**5**).*

To a solution of compound **4** (6.46 g, 33 mmol) in chloroform (100 mL) was added chlorosulfonic (11.5 g, 99 mmol) dropwise at 0 ˚C for 10 min. The reaction mixture was heated at 50 ˚C for 6 h. The mixture was then poured into ice water. The reaction mixture was extracted with DCM (150 mL×2). The organic layer was washed with brine and dried over Na_2SO_4. The solid was filtered off, and the filtrate was concentrated under reduced pressure. The resulting crude product was purified by silica gel chromatography with petroleum ether/ethyl acetate (5/1, v/v) to yield the title product as a yellow solid (5.75 g, 59%). MS (ESI), m/z for $C_{13}H_{10}ClNO_3S$ ($[M + H]^+$): Calcd 295.01, found 296.0.

*4.3.5. 1-ethyl-N-(isoquinolin-7´-yl)-2-oxo-1,2-dihydrobenzo[cd]indole-6-sulfonamide (**6f**).*

A reaction mixture of compound **5** (70 mg, 0.237 mmol) and isoquinolin-7-amine (68 mg, 0.473 mmol) in pyridine (4 mL) was stirred at room temperature overnight. Water was added, the aqueous layer was extracted with ethyl acetate (50 mL×3), and the organic layer was washed with water and brine, dried with Na_2SO_4 and evaporated. The residue was purified by silica gel chromatography with petroleum ether/ethyl acetate (2/1, v/v) to afford **6f** (76 mg, 96%) as a yellow solid. ^{1}H-NMR (400 MHz, DMSO-d_6) δ 11.04 (s, 1H, SO_2NH), 9.15 (s, 1H, 8´-H), 8.74 (d, *J* = 8.4 Hz, 1H, 5-H), 8.32 (d, *J* = 5.6 Hz, 1H, 7-H), 8.29 (d, *J* = 8.0 Hz, 1H, Ar-H), 8.09 (d, *J* = 7.2 Hz, 1H, 3-H), 7.93 (t, *J* = 7.6 Hz, 1H, 4-H), 7.78 (d, *J* = 8.8 Hz, 1H, Ar -H), 7.72 (s, 1H, Ar -H), 7.62 (d, *J* = 6.0 Hz, 1H, Ar -H), 7.47 (d, *J* = 9.2 Hz, 1H, Ar -H), 7.23 (d, *J* = 8.0 Hz, 1H, 8-H), 3.84 (q, *J* = 7.2 Hz, 2H, CH_2), 1.18 (t, *J* = 7.2 Hz, 3H, CH_3). ^{13}C-NMR (500 MHz, DMSO-d_6) δ 167.57, 152.46, 144.42, 142.79, 137.32, 134.77, 132.63, 131.69, 129.91, 129.39, 128.90, 128.22, 126.98, 126.17, 125.76, 124.84, 124.80, 120.78, 114.67, 104.85, 35.50, 14.47. MS (ESI), m/z for $C_{22}H_{17}N_3O_3S$ ([M - H]$^-$): Calcd 403.45, found 402.0.

*4.3.6. 1-ethyl-N-(4´-morpholinophenyl)-2-oxo-1,2-dihydrobenzo[cd]indole-6-sulfonamide (**7a**).*

To a solution of compound **5** (100 mg, 0.338 mmol) and 4-morpholinoaniline (84 mg, 0.473 mmol) in THF (10 mL) and acetone (10 mL) was added 2,6-lutidine (1 mL), and the reaction mixture was stirred at room temperature overnight. Water was added, and the aqueous layer was extracted with ethyl acetate (50 mL×3). The organic layer was washed with brine, dried with Na_2SO_4 and evaporated. The residue was purified by silica gel chromatography with petroleum ether/ethyl acetate (2/1, v/v) to afford **7a** (79 mg, 53%) as a yellow solid. ^{1}H-NMR (400 MHz, DMSO-d_6) δ 10.08(s, 1H, SO_2NH), 8.65 (d, *J* = 8.4 Hz, 1H, 5-H), 8.11 (d, *J* = 6.8 Hz, 1H, 7-H), 8.00 (d, *J* = 7.6 Hz, 1H, 3-H), 7.86 (t, *J* = 8.4 Hz, 1H, 4-H), 7.20 (d, *J* = 7.6 Hz, 1H, 8-H), 6.87 (d, *J* =

8.8 Hz, 2H, Ar-H), 6.70 (d, *J* = 9.2 Hz, 2H, Ar-H), 3.87 (q, *J* = 6.8 Hz, 2H, CH_2), 3.62 (m, 4H, 2´-H), 2.91 (m, 4H, 3´-H), 1.22 (t, *J* = 7.2 Hz, 3H, CH_3). ^{13}C-NMR (500 MHz, DMSO-d_6) δ 167.63, 149.16, 143.91, 133.95, 131.34, 130.31, 129.54, 129.20, 126.88, 126.02, 125.65, 125.06, 123.45, 116.39, 104.90, 66.88, 49.32, 35.51, 14.54. MS (ESI), m/z for $C_{23}H_{23}N_3O_4S$ ([M - H]$^-$): Calcd 437.51, found 436.0.

4.3.7.

*(E)-1-ethyl-2-oxo-N-(4´-(phenyldiazenyl)phenyl)-1,2-dihydrobenzo[cd]indole-6-sulfonamide (**7k**).*

A reaction mixture of compound **5** (70 mg, 0.237 mmol) and (E)-4- (phenyldiazenyl) aniline (111 mg, 0.473 mmol) in pyridine (4 mL) was stirred at room temperature overnight. Water was added, and the aqueous layer was extracted with ethyl acetate (50 mL×3). The organic layer was washed with water and brine, dried with Na_2SO_4 and evaporated. The residue was purified by silica gel chromatography with petroleum ether/ethyl acetate (2/1, v/v) to afford **7k** (51 mg, 47%) as a yellow solid. ^{1}H-NMR (400 MHz, DMSO-d_6) δ 11.10 (s, 1H, SO_2NH), 8.74 (d, *J* = 8.4 Hz, 1H, 5-H), 8.26 (d, *J* = 7.6 Hz, 1H, 7-H), 8.11 (d, *J* = 7.2 Hz, 1H, 3-H), 7.95 (t, *J* = 7.8 Hz, 1H, 4-H), 7.73 (m, *J* = 9.0 Hz, 4H, 8-H, Ar-H), 7.50 (m, 3H, Ar-H), 7.27 (m, 3H, Ar-H), 3.86 (q, *J* = 7.2 Hz, 2H, CH_2), 1.20 (t, *J* = 7.2 Hz, 3H, CH_3). ^{13}C NMR (500 MHz, DMSO-d_6) δ 167.30, 152.77, 148.68, 144.24, 141.25, 134.04, 131.51, 131.26, 129.82, 129.65, 128.57, 126.78, 125.67, 124.32, 122.78, 119.86, 104.41, 35.28, 14.00. MS (ESI), m/z for $C_{25}H_{20}N_4O_3S$ ([M - H]$^-$): Calcd 456.52, found 455.1.

4.3.8.

*Tert-butyl(3´-(1-ethyl-2-oxo-1,2-dihydrobenzo[cd]indole-6-sulfonamido)phenyl)carbamate (**8a**).*

To a solution of compound **5** (60 mg, 0.203 mmol), DAMP (5 mg, 0.041 mmol) and *tert*-butyl(3-aminophenyl)carbamate (85 mg, 0.406 mmol) in DMF (10 mL) was added TEA (0.08 mL, 0.61 mmol), and the reaction mixture was stirred at room

temperature overnight. Water was added, and the aqueous layer was extracted with ethyl acetate (50 mL×3). The organic layer was washed with brine, dried with Na_2SO_4 and evaporated. The residue was purified by silica gel chromatography with petroleum ether/ethyl acetate (5/1, v/v) to afford **8a** (55.3 mg, 58%) as a yellow solid. ^{1}H-NMR (400 MHz, $CDCl_3$) δ 8.58 (d, *J* = 8.4 Hz, 1H, 5-H), 8.17 (d, *J* = 8.0 Hz, 1H, 7-H), 8.00 (d, *J* = 7.2 Hz, 1H, 3-H), 7.68 (t, *J* = 7.6 Hz, 1H, 4-H), 7.17 (s, 1H, 2´-H), 7.01 (m, 2H, 8-H, 5´-H), 6.83 (d, *J* = 7.6 Hz, 1H, Ar-H), 6.73 (d, *J* = 7.2 Hz, 1H, Ar-H), 6.63 (s, 1H, CONH), 3.91 (q, *J* = 7.0 Hz, 2H, CH_2), 1.43 (s, 9H, $C(CH_3)_3$), 1.25 (t, *J* = 7.0 Hz, 3H, CH_3). ^{13}C-NMR (400 MHz, DMSO-d_6) δ 167.66, 153.44, 144.16, 141.12, 138.83, 134.48, 131.51, 130.20, 130.03, 128.83, 126.96, 126.07, 125.76, 124.96, 114.38, 113.77, 109.99, 104.84, 79.98, 35.52, 28.97, 14.54. MS (ESI), m/z for $C_{24}H_{25}N_3O_5S$ ($[M - H]^-$): Calcd 467.15, found 466.1.

*4.3.9. N-(4´-acetylphenyl)-1-ethyl-2-oxo-1,2-dihydrobenzo[cd]indole-6-sulfonamide (**8c**).*

To a solution of compound **5** (100 mg, 0.338 mmol) and 1-(4-aminophenyl) ethanone (64 mg, 0.473 mmol) in THF (10 mL) and 10 mL acetone (10 mL), and the reaction mixture was stirred at room temperature overnight. Water was added, and the aqueous layer was extracted with ethyl acetate (50 mL×3). The organic layer was washed with brine, dried with Na_2SO_4 and evaporated. The residue was purified by silica gel chromatography with petroleum ether/ethyl acetate (5/1, v/v) to afford **8c** (90 mg, 67%) as a yellow solid. ^{1}H-NMR (400 MHz, DMSO-d_6) δ 10.82 (s, 1H, SO_2NH), 8.69 (d, *J* = 8.4 Hz, 1H, 5-H), 8.19 (d, *J* = 7.6 Hz, 1H, 7-H), 8.09 (d, *J* = 7.2 Hz, 1H, 3-H), 7.94 (t, *J* = 8.0 Hz, 1H, 4-H), 7.57 (m, 2H, 3´-H, 5´-H), 7.31 (d, *J* = 5.6 Hz, 2H, 2´-H, 6´-H), 7.25 (d, *J* = 7.6 Hz, 1H, 8-H), 3.86 (q, *J* = 6.8 Hz, 2H, CH_2), 2.43 (s, 3H, $COCH_3$), 1.22 (t, *J* = 6.8 Hz, 3H, CH_3). ^{13}C-NMR (400 MHz, DMSO-d_6) δ 197.57, 167.30, 144.12, 138.69, 138.44, 133.81, 131.15, 130.07, 129.73, 128.68, 126.73, 125.63, 124.76, 124.55, 124.37, 119.28, 104.38, 35.26, 26.95, 13.98. MS (ESI), m/z for $C_{21}H_{18}N_2O_4S$ ($[M - H]^-$): Calcd 394.1, found 393.0.

4.3.10.

N-(2´-(tert-butyl)phenyl)-1-ethyl-2-oxo-1,2-dihydrobenzo[cd]indole-6-sulfonamide ***(8i).***

A reaction mixture of compound **5** (100 mg, 0.338 mmol) and 2-(tert-butyl) aniline (92 mg, 0.617 mmol) in pyridine (4 mL) was stirred at room temperature overnight. Water was added, and the aqueous layer was extracted with ethyl acetate (50 mL×3). The organic layer was washed with water and brine, dried with Na_2SO_4 and evaporated. The residue was purified by silica gel chromatography with petroleum ether/ethyl acetate (5/1, v/v) to afford **6i** (50 mg, 36%) as a yellow solid. ^{1}H-NMR (400 MHz, DMSO-d_6) δ 9.37(s, 1H, SO_2NH), 8.76 (d, *J*=8.4 Hz, 1H, 5-H), 8.21 (d, *J* = 7.2 Hz, 1H, 7-H), 8.05 (d, *J* = 7.6 Hz, 1H, 3-H), 7.94 (t, *J* = 8.0 Hz, 1H, 4-H), 7.44 (d, *J* = 8.0 Hz, 1H, 8-H), 7.32 (d, *J* = 7.6 Hz, 1H, Ar-H), 7.15 (t, *J* = 7.6 Hz, 1H Ar-H), 6.90 (t, *J* = 7.6 Hz, 1H, Ar-H), 6.36 (d, *J* = 7.6 Hz, 1H, Ar-H), 3.97 (q, *J* = 7.2 Hz, 2H, CH_2), 1.45 (s, 9H, $C(CH_3)$), 1.29 (t, *J* = 7.2 Hz, 3H, CH_3). ^{13}C-NMR (400 MHz, DMSO-d_6) δ 167.48, 148.58, 143.62, 134.99, 132.94, 131.90, 130.79, 130.72, 129.92, 128.31, 127.92, 126.72, 126.65, 125.71, 125.52, 124.96, 104.59, 35.90, 35.31, 32.28, 14.05. MS (ESI), m/z for $C_{23}H_{24}N_2O_3S$ ($[M - H]^-$): Calcd 408.15, found 407.1.

4.3.11.

N-(3´,4´-dimethoxyphenyl)-1-ethyl-2-oxo-1,2-dihydrobenzo[cd]indole-6-sulfonamide ***(8k).***

To a solution of compound **5** (70 mg, 0.237 mmol), DAMP (6 mg, 0.047 mmol) and 3,4-dimethoxyaniline (73 mg, 0.473 mmol) in DMF (10 mL) was added TEA (0.1 mL, 0.71 mmol), and the reaction mixture was stirred at room temperature overnight. Water was added, and the aqueous layer was extracted with ethyl acetate (50 mL×3). The organic layer was washed with brine, dried with Na_2SO_4 and evaporated. The residue was purified by silica gel chromatography with petroleum ether/ethyl acetate (5/1, v/v) to afford **8k** (47.6 mg, 49%) as a yellow solid. ^{1}H-NMR (400 MHz, $CDCl_3$) δ 8.55 (d, *J* = 8.4 Hz, 1H, 5-H), 8.04 (t, *J* = 3.6 Hz, 2H, 7-H, 3-H), 7.72 (t, *J* = 7.4 Hz, 1H, 4-H), 6.82 (d, *J* = 7.6 Hz, 1H, 8-H), 6.64 (s, 1H, 2´-H), 6.55 (d, *J* = 8.8 Hz, 1H,

5´-H), 6.41 (d, *J* = 8.4 Hz, 1H, 6´-H), 3.93 (q, *J* = 7.0 Hz, 2H, CH_2), 3.73 (s, 3H, OCH_3), 3.65 (s, 3H, OCH_3), 1.24 (t, *J* = 7.0 Hz, 3H, CH_3). ^{13}C-NMR (400 MHz, DMSO-d_6) δ 167.39, 149.74, 147.09, 143.83, 133.68, 131.20, 130.98, 130.08, 129.12, 126.70, 125.58, 125.00, 114.47, 113.56, 104.49, 56.61, 56.29, 35.29, 14.08. MS (ESI), m/z for $C_{21}H_{20}N_2O_5S$ ([M - H]$^-$): Calcd 412.46, found 411.1.

4.3.12.

N-(2´,5´-dichlorobenzyl)-1-ethyl-2-oxo-1,2-dihydrobenzo[cd]indole-6-sulfonamide ***(8s)****.*

To a solution of compound **5** (100 mg, 0.338 mmol) and (2,5-dichlorophenyl) methanamine (72 mg, 0.409 mmol) in DCM (10 mL) was added DIPEA (1 mL), and the reaction mixture was stirred at room temperature overnight. Water was added, and the aqueous layer was extracted with ethyl acetate (50 mL×3). The organic layer was washed with brine, dried with Na_2SO_4 and evaporated. The residue was purified by silica gel chromatography with petroleum ether/ethyl acetate (3/1, v/v) to afford **6s** (32 mg, 21%) as a yellow solid. ^{1}H-NMR (400 MHz, DMSO-d_6) δ 8.68 (d, *J* = 8.4 Hz, 1H, 5-H), 8.28 (t, *J* = 5.2 Hz, 1H, 7-H), 8.11 (m, 1H, 3-H), 7.88 (t, *J* = 8.0 Hz, 1H, 4-H), 7.26 (d, *J* = 7.6 Hz, 1H, 8-H), 7.19 (d, *J* = 7.2 Hz, 2H, Ar-H), 7.13 (m, 1H, Ar-H), 4.25 (d, *J* = 5.2 Hz, 2H, $ArCH_2$) , 3.93 (q, *J* = 7.2 Hz, 2H, CH_2), 1.27 (t, *J* = 7.2 Hz, 3H, CH_3). ^{13}C-NMR (400 MHz, DMSO-d_6) δ 167.48, 143.54, 135.99, 133.09, 132.42, 130.72, 130.57, 130.50, 128.83, 126.53, 125.40, 124.97, 104.32, 42.20, 35.25, 14.13. MS (ESI), m/z for $C_{20}H_{16}Cl_2N_2O_3S$ ([M - H]$^-$): Calcd 434.03, found 433.0.

4.4. Biological assays

4.4.1. Protein and peptide preparation

The human RORγ LBD (residues 262–507) was expressed as a His6-fusion protein using the pET24a expression vector (Novagen, Madison, WI) as described in reference [23]. BL21 (DE3) cells that were transformed with this expression plasmid were grown in LB broth at 25 ˚C until an OD_{600} of approximately 1.0 was reached, and the cells were then induced with 0.1 mM isopropyl-β-D-1-thiogalactopyranoside

(IPTG) at 16 ˚C overnight. Cells were harvested, resuspended, and high-pressure homogenized in 200 mL of extract buffer (20 mM Tris (pH 8.0), 500 mM NaCl, 10% glycerol, and 25 mM imidazole) per 6 liters of cells. The lysate was centrifuged at 20,000 rpm for 30 min, and the supernatant was loaded onto a 5-mL $NiSO_4$-loaded HisTrap HP column (GE Healthcare, Piscataway, NJ). The column was washed with extract buffer, and the protein was eluted with a 25–500 mM imidazole gradient. A gel filtration column (HiLoad S75, 16/60, GE Healthcare) was used for a second purification.

4.4.2. AlphaScreen assays

Interactions between RORγ and ligands were assessed by luminescence-based AlphaScreen technology (Perkin Elmer) as previously described in [22-25] using a histidine detection kit from PerkinElmer (Norwalk, CT). All of the reactions contained 100 nM receptor LBD bound to nickel acceptor beads (5 μg/mL) and 20 nM biotinylated SRC1-4 peptide bound to streptavidin donor beads (5 μg/mL) in the presence or absence of the indicated amounts of control compounds T0901317, UA, SR2211, or candidate compounds. The N-terminal biotinylated coactivator peptide SRC1-4 sequence was QKPTSGPQTPQAQQKSLLQQLLTE. Compound concentrations varied from 150 nM to 200 μM in the dose-response assay.

4.4.3. Transient transfection assays

293T cells were maintained in DMEM containing 10% fetal bovine serum (FBS). Cells were transiently transfected in Opti-MEM using Lipofectamine 2000 (Invitrogen), according to the manufacturer's protocol. The 96-well plates were plated 24 h prior to transfection (15000 cells per well). For all of the experiments, each well of cells was transfected in Opti-MEM with 25 ng of reporter plasmids and 5 ng of Renilla luciferase expression plasmids. For Gal4-driven reporter assays, the cells were transfected with 25 ng of Gal4-RORγ LBD (residues 262-507) and 25 ng of pG5Luc reporter. For native promoter reporter assays, the cells were co-transfected with the Pcp2/RORE-Luc reporter along with the plasmids encoding full-length RORγ. The

cells were then transfected with the indicated expression and reporter plasmids. The media was changed 24 h after transfection, and the compounds were added. Cells were incubated for another 24 h followed by harvesting for a luciferase assay using the dual-luciferase reporter assay system (Promega). Luciferase data were normalized to Renilla luciferase data, which was used as an internal transfection control. All of the assays were performed in triplicate, and the standard deviations were calculated using the triplicates.

Acknowledgements

We gratefully acknowledge financial support from the National Natural Science Foundation of China (Grant 81373325), National Key Basic Research Program of China (973 Program, Grant 2013CB910601), the “100 Talents Project” of CAS, and Guangzhou Bureau of Science and Information Technology, China, (Grants 2012Y2-00051, 2013Y2-00048),“Interdisciplinary Cooperation Team” Program for Science and Technology Innovation of the CAS. We gratefully thank Professor Yong Li for advice and related plasmids.

Appendix A. Supplementary material

Supplementary data associated with this article can be found, in the online version, at doi:xxx.

Figure Legends

Figure 1. Selected examples of known RORγ antagonists as disclosed in the literature and RORγ virtual screening hit (**s4**).

Figure 2. Schematic representation of the virtual screening workflow used for RORγ ligand discovery in this study.

Figure 3. 3D (A) and 2D (B) schematic presentation of the predicted binding mode of **s4** in the RORγ ligand binding pocket.

Figure 4. 3D presentation of the predicted binding modes of **7j** (A), **8c** (B), **8k** (C), **8p** (D) in the RORγ ligand binding pocket.

Table 1. SAR of the sulfonamide with a fused heterocyclic ring.

Table 2. SAR of the sulfonamide with multiple ring substituents.

Table 3. SAR of the sulfonamide with a single ring substituent.

References

[1] D.R. Littman, and A.Y. Rudensky. Th17 and regulatory T cells in mediating and restraining inflammation. Cell. 140 (2010) 845-858

[2] Ivanov, II, L. Zhou, and D.R. Littman. Transcriptional regulation of Th17 cell differentiation. Semin Immunol. 19 (2007) 409-417

[3] X.O. Yang, R. Nurieva, G.J. Martinez, H.S. Kang, Y. Chung, B.P. Pappu, B. Shah, S.H. Chang, K.S. Schluns, S.S. Watowich, X.H. Feng, A.M. Jetten, and C. Dong. Molecular antagonism and plasticity of regulatory and inflammatory T cell programs. Immunity. 29 (2008) 44-56

[4] L.A. Solt, and T.P. Burris. Action of RORs and their ligands in (patho)physiology. Trends Endocrinol Metab. 23 (2012) 619-627

[5] N. Kumar, L.A. Solt, J.J. Conkright, Y. Wang, M.A. Istrate, S.A. Busby, R.D. Garcia-Ordonez, T.P. Burris, and P.R. Griffin. The benzenesulfoamide T0901317 [N-(2,2,2-trifluoroethyl)-N-[4-[2,2,2-trifluoro-1-hydroxy-1-(trifluoromethyl)ethy l]phenyl]-benzenesulfonamide] is a novel retinoic acid receptor-related orphan receptor-alpha/gamma inverse agonist. Mol Pharmacol. 77 (2010) 228-236

[6] T.M. Kamenecka, B. Lyda, M.R. Chang, and P.R. Griffin. Synthetic modulators of the retinoic acid receptor-related orphan receptors. MedChemComm. 4 (2013) 764-776

[7] J.R. Huh, and D.R. Littman. Small molecule inhibitors of RORgammat: targeting Th17 cells and other applications. Eur J Immunol. 42 (2012) 2232-2237

[8] J.R. Huh, M.W. Leung, P. Huang, D.A. Ryan, M.R. Krout, R.R. Malapaka, J. Chow, N. Manel, M. Ciofani, S.V. Kim, A. Cuesta, F.R. Santori, J.J. Lafaille, H.E. Xu, D.Y. Gin, F. Rastinejad, and D.R. Littman. Digoxin and its derivatives suppress TH17 cell differentiation by antagonizing RORgammat activity. Nature. 472 (2011) 486-490

[9] S. Fujita-Sato, S. Ito, T. Isobe, T. Ohyama, K. Wakabayashi, K. Morishita, O. Ando, and F. Isono. Structural basis of digoxin that antagonizes RORgamma t receptor activity and suppresses Th17 cell differentiation and interleukin (IL)-17 production. J Biol Chem. 286 (2011) 31409-31417

[10] T. Xu, X. Wang, B. Zhong, R.I. Nurieva, S. Ding, and C. Dong. Ursolic acid suppresses interleukin-17 (IL-17) production by selectively antagonizing the function of RORgamma t protein. J Biol Chem. 286 (2011) 22707-22710

[11] L.A. Solt, N. Kumar, P. Nuhant, Y. Wang, J.L. Lauer, J. Liu, M.A. Istrate, T.M. Kamenecka, W.R. Roush, D. Vidovic, S.C. Schurer, J. Xu, G. Wagoner, P.D. Drew, P.R. Griffin, and T.P. Burris. Suppression of TH17 differentiation and autoimmunity by a synthetic ROR ligand. Nature. 472 (2011) 491-494

[12] N. Kumar, B. Lyda, M.R. Chang, J.L. Lauer, L.A. Solt, T.P. Burris, T.M. Kamenecka, and P.R. Griffin. Identification of SR2211: a potent synthetic RORgamma-selective modulator. ACS Chem Biol. 7 (2012) 672-677

[13] L.A. Solt, N. Kumar, Y. He, T.M. Kamenecka, P.R. Griffin, and T.P. Burris. Identification of a selective RORgamma ligand that suppresses T(H)17 cells and stimulates T regulatory cells. ACS Chem Biol. 7 (2012) 1515-1519

[14] J.R. Huh, E.E. Englund, H. Wang, R. Huang, P. Huang, F. Rastinejad, J. Inglese, C.P. Austin, R.L. Johnson, W. Huang, and D.R. Littman. Identification of Potent and Selective Diphenylpropanamide RORgamma Inhibitors. ACS Med Chem Lett. 4 (2013) 79-84

[15] B.P. Fauber, G. de Leon Boenig, B. Burton, C. Eidenschenk, C. Everett, A. Gobbi, S.G. Hymowitz, A.R. Johnson, M. Liimatta, P. Lockey, M. Norman, W. Ouyang, O. Rene, and H. Wong. Structure-based design of substituted hexafluoroisopropanol-arylsulfonamides as modulators of RORc. Bioorg Med Chem Lett. 23 (2013) 6604-6609

[16] Y. Wang, W. Cai, G. Zhang, T. Yang, Q. Liu, Y. Cheng, L. Zhou, Y. Ma, Z. Cheng, S. Lu, Y.G. Zhao, W. Zhang, Z. Xiang, S. Wang, L. Yang, Q. Wu, L.A. Orband-Miller, Y. Xu, J. Zhang, R. Gao, M. Huxdorf, J.N. Xiang, Z. Zhong, J.D. Elliott, S. Leung, and X. Lin. Discovery of novel N-(5-(arylcarbonyl)thiazol-2-yl)amides and N-(5-(arylcarbonyl)thiophen-2-yl)amides as potent RORgammat inhibitors. Bioorg Med Chem. 22 (2014) 692-702

[17] T. Yang, Q. Liu, Y. Cheng, W. Cai, Y. Ma, L. Yang, Q. Wu, L.A. Orband-Miller, L. Zhou, Z. Xiang, M. Huxdorf, W. Zhang, J. Zhang, J.-N. Xiang, S. Leung, Y. Qiu, Z. Zhong, J.D. Elliott, X. Lin, and Y. Wang. Discovery of Tertiary Amine and Indole Derivatives as Potent RORγt Inverse Agonists. ACS Med. Chem Lett. 22 (2014) 692-702

[18] J. Shen, J. Jiang, G. Kuang, C. Tan, G. Liu, J. Huang, and Y. Tang. Discovery and structure-activity analysis of selective estrogen receptor modulators via similarity-based virtual screening. Eur J Med Chem. 54 (2012) 188-196

[19] J. Fu, P. Si, M. Zheng, L. Chen, X. Shen, Y. Tang, and W. Li. Discovery of new non-steroidal FXR ligands via a virtual screening workflow based on Phase shape and induced fit docking. Bioorg Med Chem Lett. 22 (2012) 6848-6853

[20] H. Huang, Y. Yu, Z. Gao, Y. Zhang, C. Li, X. Xu, H. Jin, W. Yan, R. Ma, J. Zhu, X. Shen, H. Jiang, L. Chen, and J. Li. Discovery and optimization of 1,3,4-trisubstituted-pyrazolone derivatives as novel, potent, and nonsteroidal farnesoid X receptor (FXR) selective antagonists. J Med Chem. 55 (2012) 7037-7053

[21] X.E. Zhou, K.M. Suino-Powell, Y. Xu, C.W. Chan, O. Tanabe, S.W. Kruse, R. Reynolds, J.D. Engel, and H.E. Xu. The orphan nuclear receptor TR4 is a vitamin A-activated nuclear receptor. J Biol Chem. 286 (2011) 2877-2885

[22] K. Suino-Powell, Y. Xu, C. Zhang, Y.G. Tao, W.D. Tolbert, S.S. Simons, Jr., and H.E. Xu. Doubling the size of the glucocorticoid receptor ligand binding pocket by deacylcortivazol. Mol Cell Biol. 28 (2008) 1915-1923

[23] L. Jin, D. Martynowski, S. Zheng, T. Wada, W. Xie, and Y. Li. Structural basis for hydroxycholesterols as natural ligands of orphan nuclear receptor RORgamma. Mol Endocrinol. 24 (2010) 923-929

[24] K. Melcher, Y. Xu, L.M. Ng, X.E. Zhou, F.F. Soon, V. Chinnusamy, K.M. Suino-Powell, A. Kovach, F.S. Tham, S.R. Cutler, J. Li, E.L. Yong, J.K. Zhu, and H.E. Xu. Identification and mechanism of ABA receptor antagonism. Nat Struct Mol Biol. 17 (2010) 1102-1108

[25] M. Cao, X. Liu, Y. Zhang, X. Xue, X.E. Zhou, K. Melcher, P. Gao, F. Wang, L. Zeng, Y. Zhao, Y. Zhao, P. Deng, D. Zhong, J.K. Zhu, H.E. Xu, and Y. Xu. An ABA-mimicking ligand that reduces water loss and promotes drought resistance in plants. Cell Res. 23 (2013) 1043-1054

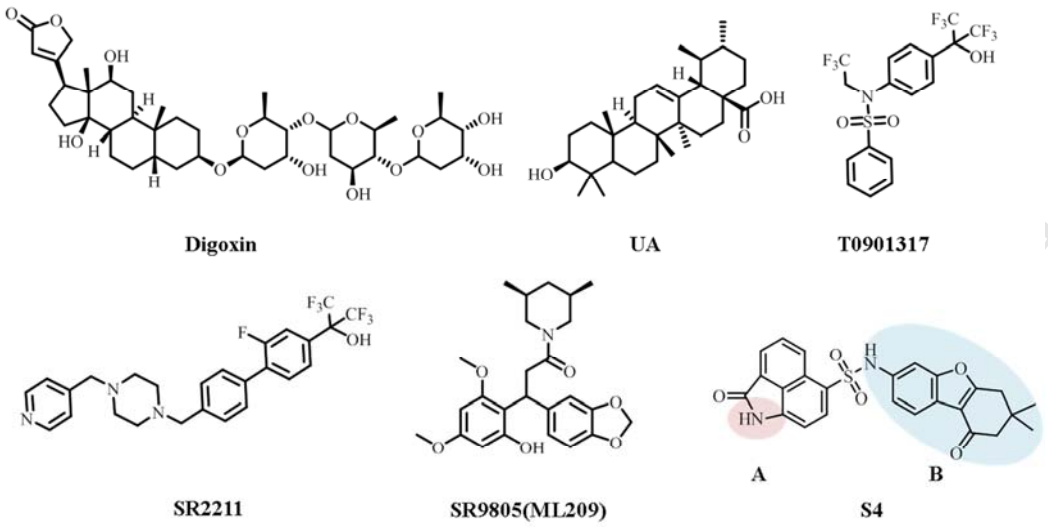

Figure 1. Selected examples of known RORγ antagonists disclosed in the literature and RORγ virtual screening hit (s4).

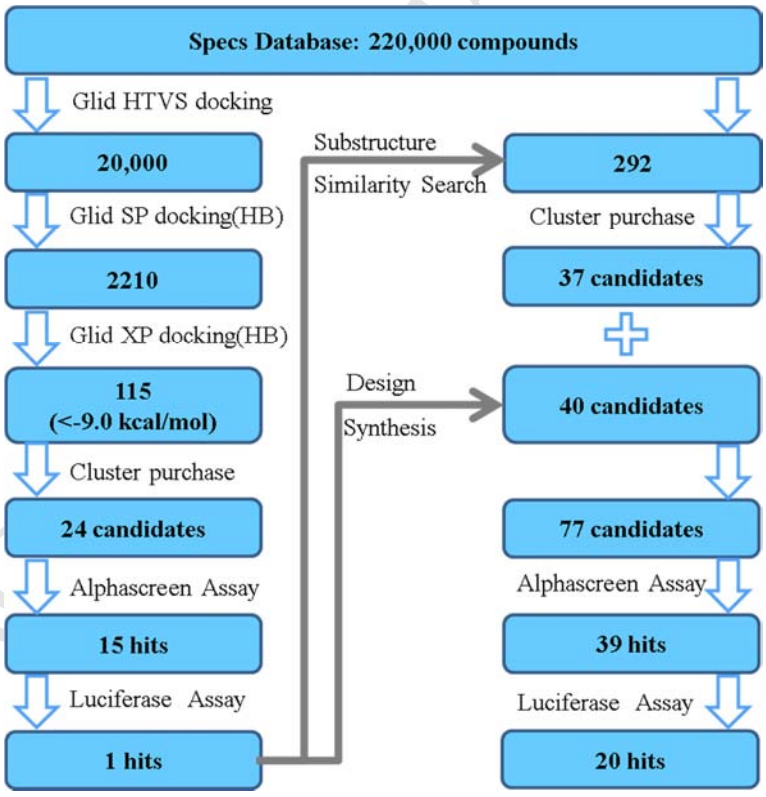

Figure 2. Schematic representation of the virtual screening workflow used for RORγ ligand discovery in this study.

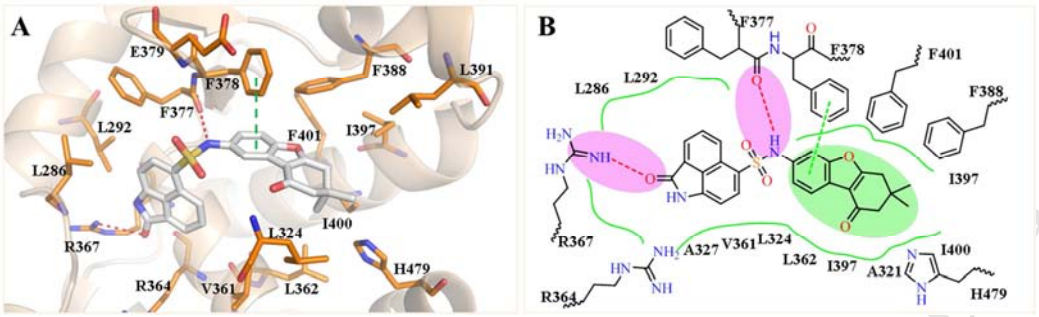

Figure 3. 3D (A) and 2D (B) schematic presentation of the predicted binding mode of s4 in RORγ ligand binding pocket. Hydrogen bonds interactions are indicated by dash lines in red, and π-π interactions indicted by dash lines in green. Fused heterocyclic ring on the right side is surrounded by hydrophobic residues Phe378, Phe388, and Phe401.

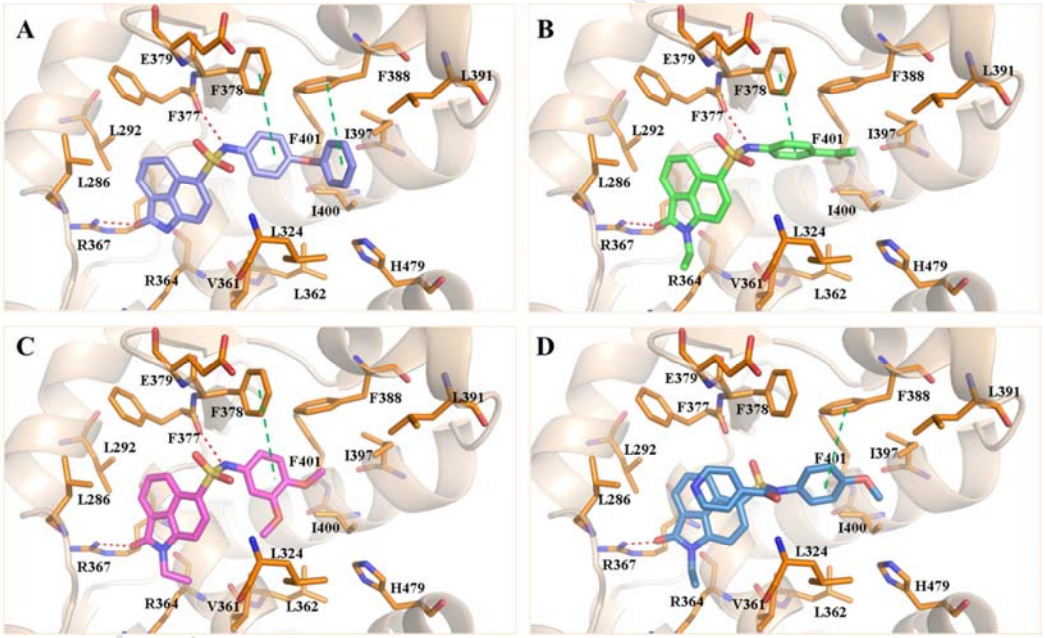

Figure 4. 3D presentation of predicted binding modes of **7j** (A), **8c** (B), **8k** (C), **8p** (D) in the RORγ ligand binding pocket. Hydrogen bonds interactions are indicated by dash lines in red, and π-π interactions indicated by dash lines in green. Aromatic ring on the right side is surrounded by hydrophobic residues Phe378, Phe388, and Phe401.

Table 1. SAR of the sulfonamide with a fused heterocyclic ring.

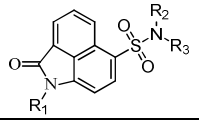

Cmpd	R_1	R_2	R_3	Luciferase		Alphascreen
				Gal4-RORγ-LBD	full-length-RORγ	RORγ-LBD
				IC_{50} (μM)[a] (%max inhibition)	IC_{50} (μM)[a] (%max inhibition)	IC_{50} (μM)[b]
T1317				0.54 (82)	3.5 (76)	2.50 ± 0.87
UA				0.13 (76)	1.06 (63)	9.41 ± 1.07
SR2211				0.43 (79)	0.42 (44)	3.54 ± 0.01
s4	H	H	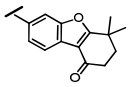	11.84 (79)	7.56 (62)	20.27 ± 6.26
6a*	Et	H	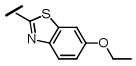	0.93 (60)	1.35 (45)	6.72 ± 0.89
6b	Et	H	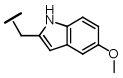	(10)	(10)	-
6c	Et	H	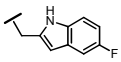	1.21 (32)	12.76 (34)	-
6d	Et	H		(30)	(20)	-
6e	Et	H	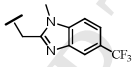	(20)	(40)	-
6f	Et	H		0.10 (70)	0.15 (72)	17.52 ± 4.07
6g*	Et	H		(40)	(10)	14.09 ± 2.07
6h*	H	H	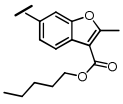	(10)	(20)	23.77 ± 4.35
6i	Et	H	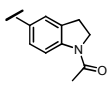	(40)	(40)	52.26 ± 4.21

[a] Inhibition of constitutive activity of RORγ by tested compounds.

[b] Inhibition of RORγ LBD recruitment of the SRC1-4 coactivator peptide.

* Denotes compounds from similarity/substructure search.

Table 2. SAR of the sulfonamide with multiple ring substituents.

Cmpd	R_1	R_2	R_3	Luciferase		Alphascreen
				Gal4-RORγ-LBD	full-length-RORγ	RORγ-LBD
				IC_{50} (μM)[a] (%max inhibition)	IC_{50} (μM)[a] (%max inhibition)	IC_{50} (μM)[b]
7a	Et	H	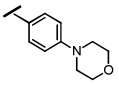	0.34 (60)	0.55 (71)	12.15 ± 0.05
7b*	H	H	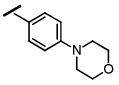	0.30 (64)	0.41 (54)	48.42 ± 2.93
7c	Et	H	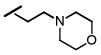	0.35 (63)	0.29 (63)	-
7d	Et	H	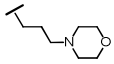	(10)	(30)	-
7e*	H	H	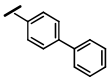	(20)	(40)	5.93 ± 0.07
7f	Et	H	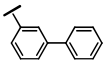	(53)	(58)	-
7g*	Et	H	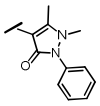	(10)	(20)	-
7h	Et	H	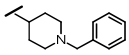	(50)	(50)	-
7i	Et	H	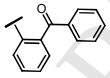	(20)	(30)	156.30 ± 8.7
7j*	H	H	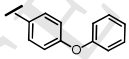	0.14 (70)	0.15 (60)	3.09 ± 0.71
7k	Et	H	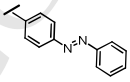	0.20 (59)	0.2 (54)	6.05 ± 1.09
7m*	H	H	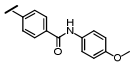	0.38 (65)	0.18 (60)	8.35 ± 0.45

[a] Inhibition of constitutive activity of RORγ by tested compounds.

[b] Inhibition of RORγ LBD recruitment of the SRC1-4 coactivator peptide.

[*] Denotes compounds from similarity/substructure search.

Table 3. SAR of the sulfonamide with a single ring substituent.

Cmpd	R_1	R_2	R_3	Luciferase		Alphascreen
				Gal4-RORγ-LBD	full-length-RORγ	RORγ-LBD
				IC_{50} (μM)[a] (%max inhibition)	IC_{50} (μM)[a] (%max inhibition)	IC_{50} (μM)[b]
8a	Et	H	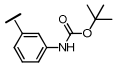	2.51 (79)	3.39 (80)	7.04 ± 1.20
8b	Et	H	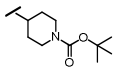	(50)	-	-
8c	Et	H	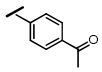	0.04 (75)	0.05 (64)	70.14 ± 4.39
8d	Et	H		0.27 (44)	0.09 (73)	-
8e	Et	H	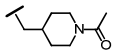	6.03 (44)	0.59 (27)	-
8f	Et	H		(10)	(30)	-
8g	Et	H	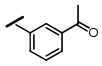	0.01 (67)	0.04 (62)	-
8h*	Et	H	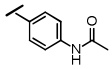	0.32 (65)	0.09 (67)	89.76 ± 1.27
8i	Et	H		4.90 (70)	9.98 (65)	18.98 ± 3.71
8j	Et	H		(10)	(20)	13.22 ± 3.21
8k	Et	H		0.05 (72)	0.02 (71)	20.10 ± 1.53
8m	Et	H	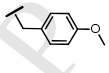	(30)	(30)	174.40
8n*	Et	H	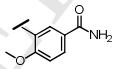	(10)	(10)	-
8p*	Et		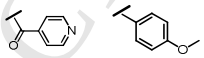	0.09 (70)	0.08 (55)	6.47 ± 0.84
8q	Et	H	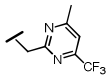	2.57 (62)	0.41 (67)	-
8r	Et	H		(40)	(40)	-
8s	Et	H		0.13 (66)	1.08 (53)	31.61 ± 2.14
8t	Et	H		(40)	(50)	-

8u	Et	H	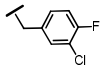	(30)	(40)	-

[a] Inhibition of constitutive activity of RORγ by tested compounds.
[b] Inhibition of RORγ LBD recruitment of the SRC1-4 coactivator peptide.
[*] Denotes compounds from similarity/substructure search.

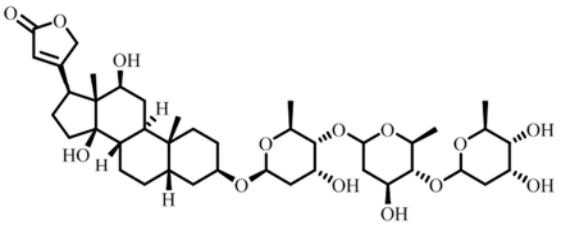

Digoxin

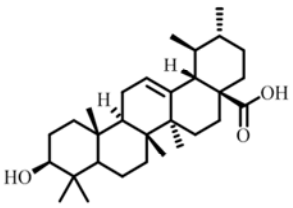

UA

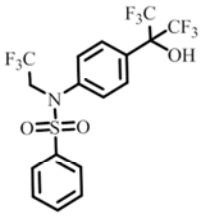

T0901317

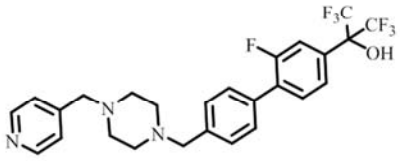

SR2211

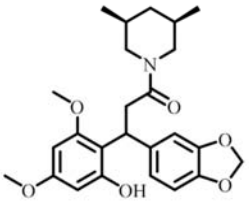

SR9805(ML209)

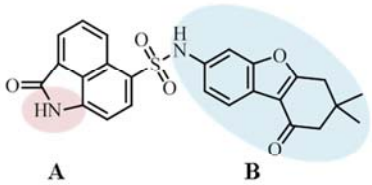

A **B**

S4

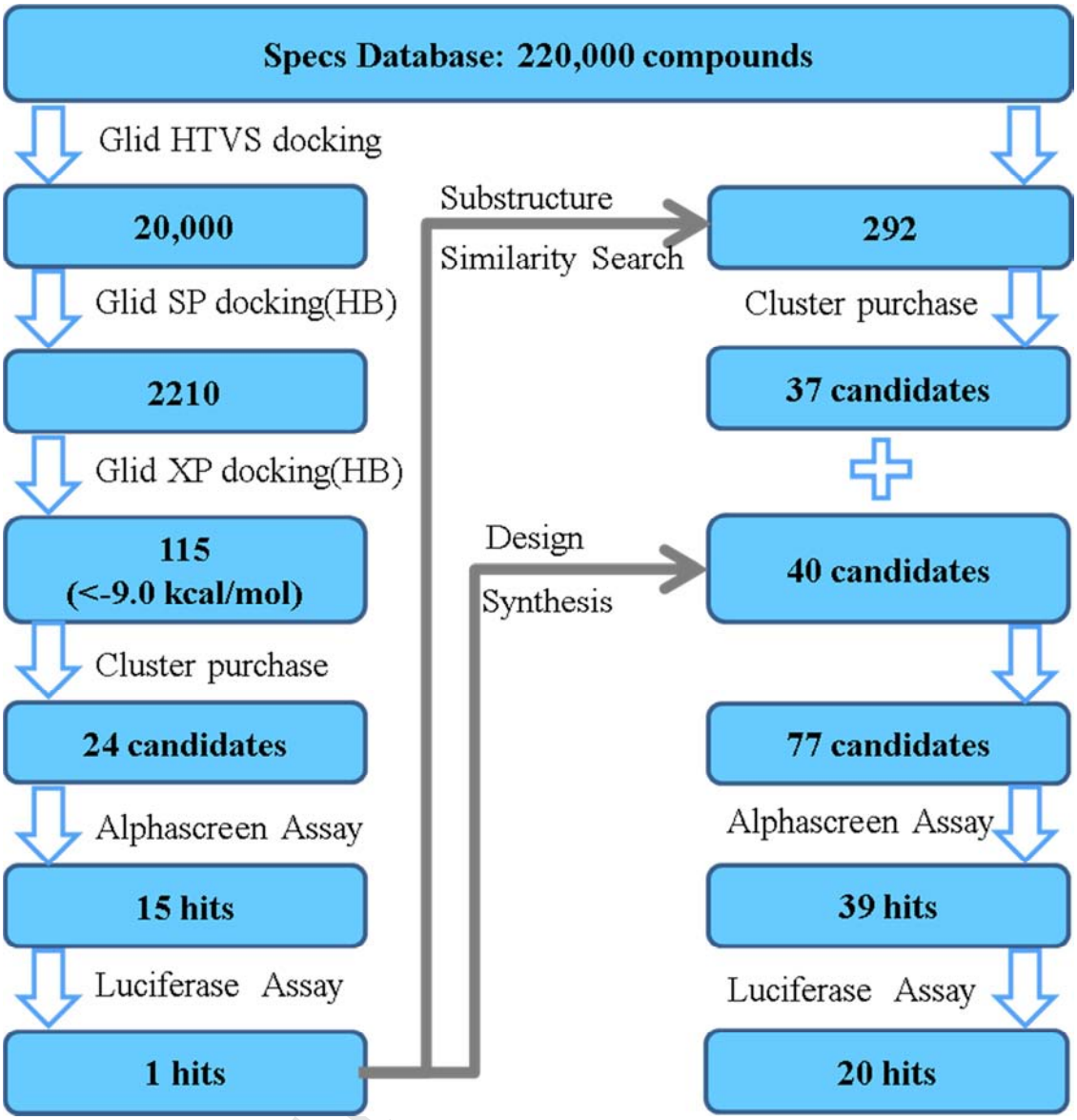
Specs Database: 220,000 compounds
Glid HTVS docking
20,000
Glid SP docking(HB)
2210
Glid XP docking(HB)
115
(<-9.0 kcal/mol)
Cluster purchase
24 candidates
Alphascreen Assay
15 hits
Luciferase Assay
1 hits
Substructure
Similarity Search
292
Cluster purchase
37 candidates
Design
Synthesis
40 candidates
77 candidates
Alphascreen Assay
39 hits
Luciferase Assay
20 hits

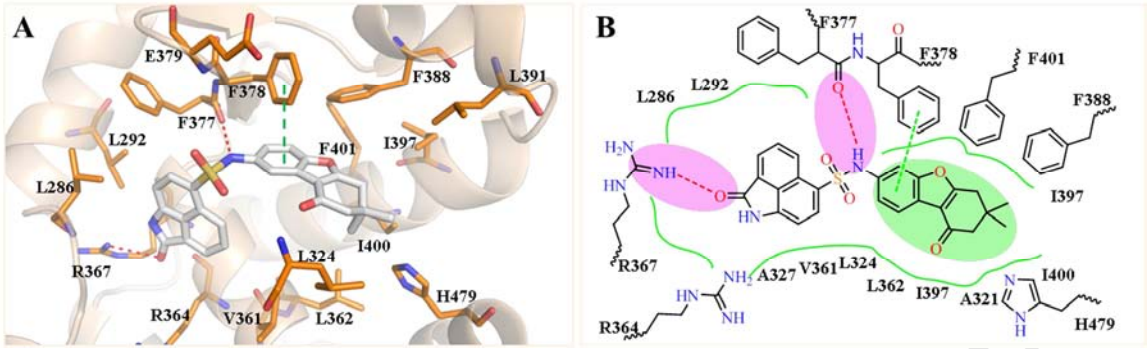

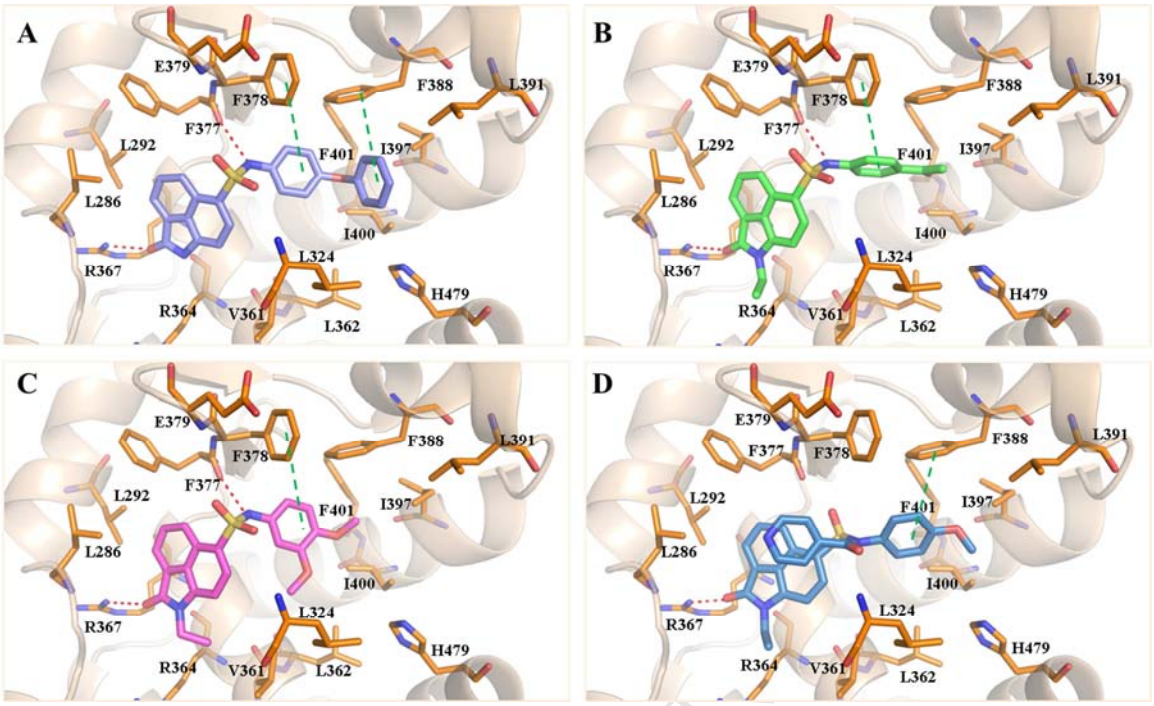

Supplementary Materials:

Supplementary Table 1. Supplier information, Glide XP GScores, and ranking for each of the assessed compounds.

Supplementary Table 2. Suppression of constitutive activity of RORγ by virtually screened compounds and reference ligands.

Supplementary Figure S1. 2D structures of the first round hit compounds from virtual screening.

Supplementary Figure S2: Single point activity result for the screened compounds at 50 μM using the AlphaScreen assay.

Supplementary Figure S3: Predicted binding modes of additional ligands with the LBD.

Supplementary Figure S4: Dose-response curves for suppression of constitutive activity of RORγ by T1317, **7j**, **8c**, **8k**, and **8p** in the AlphaScreen and reporter gene assays.

Supplementary Figure S5: ^{1}H-NMR and ^{13}C-NMR spectra of compounds **6f**, **7a**, **7k**, **8a**, **8c**, **8i**, **8k**, and **8s**.

Supplementary Table 1. Supplier information, Glide XP GScores, and ranking for each of the tested compounds.

Compound	SPECS ID	XP-GScore	Ranking	MW	AlogP
s1	AR-318/42871695	-9.09	23	364.80	2.94
s2	AK-968/15254261	-9.06	24	457.93	3.96
s3	AG-205/11218162	-10.54	4	559.41	5.35
s4	AG-690/15438001	-9.29	15	460.50	3.37
s5	AN-919/40868728	-9.26	18	565.66	4.15
s6	AG-690/40751044	-10.67	2	539.57	5.45
s7	AK-968/41170314	-9.96	8	531.51	5.10
s8	AH-487/42145080	-9.18	20	492.57	3.36
s9	AN-989/40872722	-10.61	3	540.49	2.34
s10	AK-968/40642622	-9.61	10	380.82	3.82
s11	AK-968/40709644	-9.37	13	406.84	2.90
s12	AN-329/10088022	-9.12	22	480.55	6.95
s13	AO-476/43362644	-9.15	21	463.96	3.00
s14	AN-919/41152740	-9.51	12	582.65	3.25
s15	AN-465/41377374	-9.27	17	378.79	3.43
s16	AN-919/41439252	-9.35	14	472.62	4.06
s17	AF-399/41692703	-9.80	9	590.67	2.70
s18	AG-650/41069241	-10.35	6	456.40	0.53
s19	AO-022/43453007	-9.29	16	450.89	3.37
s20	AO-022/43454460	-10.43	5	476.50	3.65
s21	AN-465/42784379	-10.73	1	430.95	4.18
s22	AN-465/43369996	-10.08	7	390.88	3.51
s23	AP-970/42224548	-9.58	11	418.31	5.07
s24	AQ-390/43363961	-9.24	19	431.49	1.54

Supplementary Table 2. Suppression of constitutive activity of RORγ by virtually screened compounds and reference ligands.

Cmpd	Alphascreen	Luciferase			
	RORγ-LBD	Gal4-RORγ-LBD		full-length-RORγ	
	IC_{50} (μM)	IC_{50} (μM)	Inhibitory rate at 10μM(%)	IC_{50} (μM)	Inhibitory rate at 10μM(%)
T1317	2.50 ± 0.87	0.54	82	3.50	76
UA	9.41 ± 1.07	0.13	76	1.06	63
SR2211	3.54 ± 0.01	0.43	79	0.42	44
s1	—	—	<10	—	<10
s2	56.64±7.74		<30		<10
s3	—	—	<10	—	<10
s4	20.27±6.26	11.84	79	7.56	77
s5	11.14±0.24	—	<40	—	<20
s6	11.64±1.19	—	<20	—	<10
s7	—	—	<10	—	<10
s8	15.17±0.77	—	<20	—	<10
s9	2.44±0.56	—	<30	—	<20
s10	168.27±8.11	—	<10	—	<10
s11	81.69±8.31	—	<20	—	<10
s12	37.54±1.41	—	<10	—	<10
s13	—	—	<30	—	<30
s14	46.87±9.37	—	<30	—	<10
s15	—	—	<20	—	<10
s16	18.27±0.34	—	<10	—	<10
s17	142.21±8.48	—	<10	—	<10
s18	—	—	<10	—	<10
s19	9.05±2.00	—	<10	—	<10
s20	—	—	<10	—	<10
s21	—	—	<10	—	<10
s22	—	—	<10	—	<10
s23	—	—	<10	—	<10
s24	—	—	<50	5.15	42

Supplementary Figure S1. 2D structures of the first round hit compounds from virtual screening.

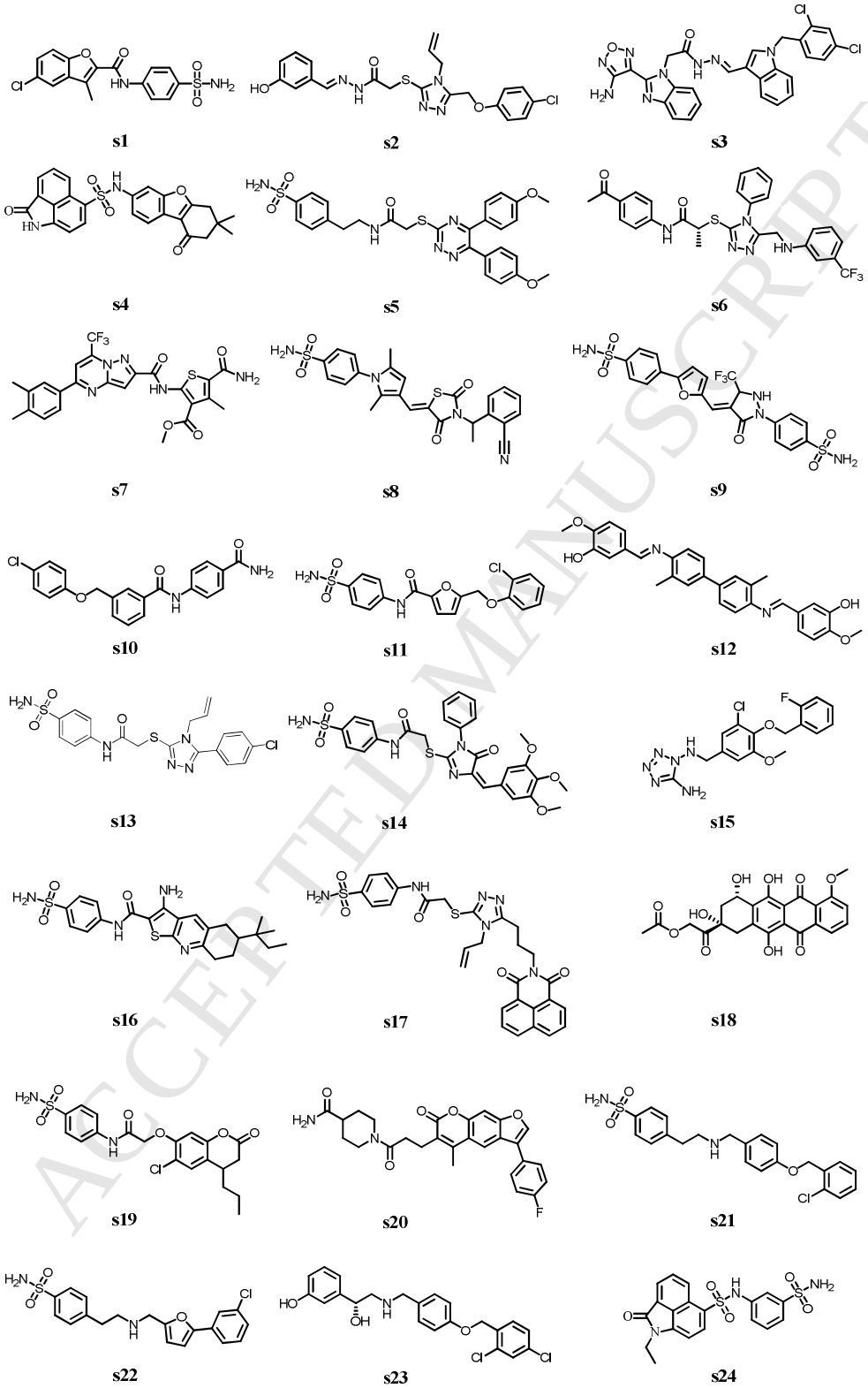

Supplementary Figure S2: Single point activity result for the screened compounds at 50 μM using the AlphaScreen assay.

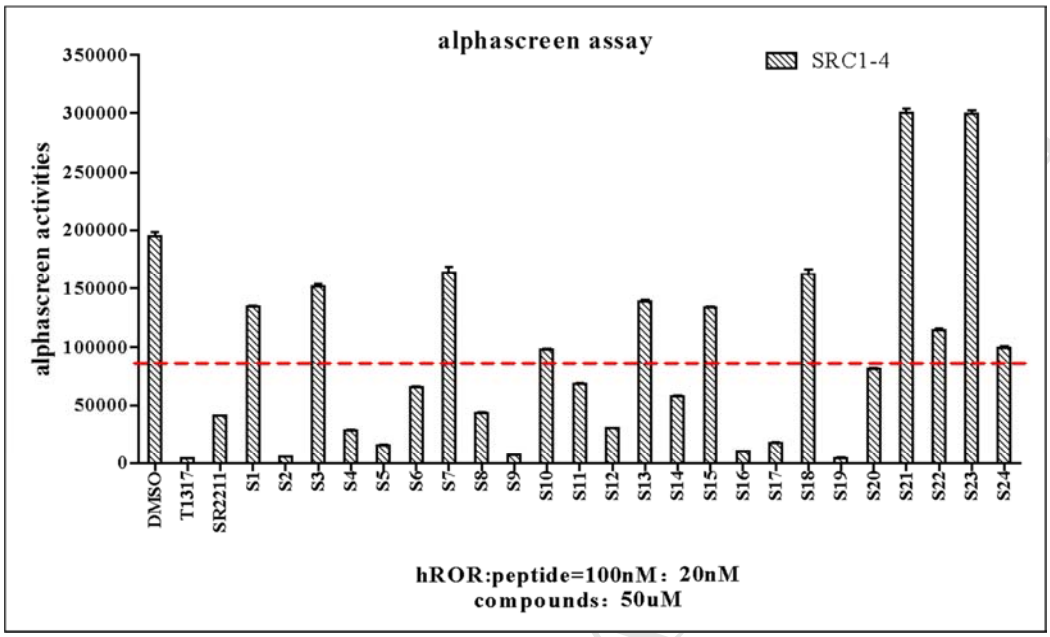

Supplementary Figure S3: Predicted binding modes of additional ligands with the RORγ LBD. (A) RORγ-**6a**, (B) RORγ-**6d**, (C) RORγ-**7a,** (D) RORγ-**7k,** (E) RORγ-**7m**, (F) RORγ-**8g.**

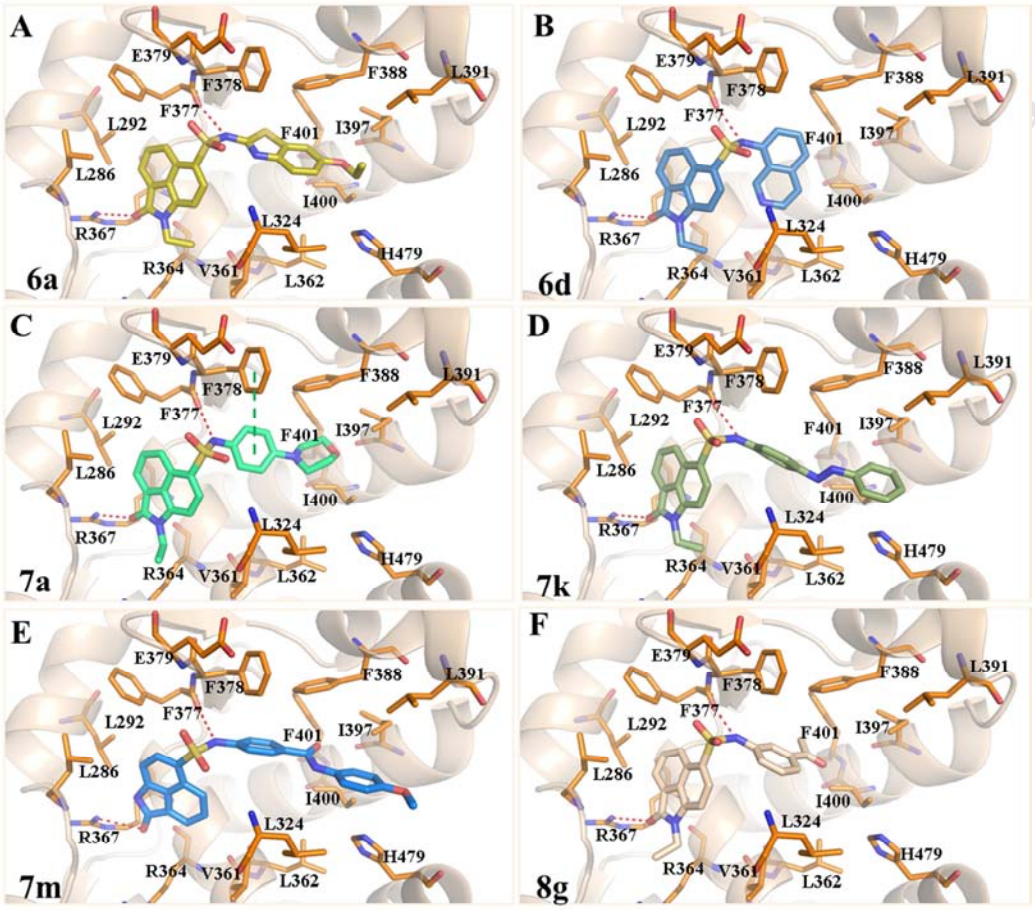

Supplementary Figure S4: Dose-response curves for suppression of constitutive activity of RORγ by T1317, **7j**, **8c**, **8k**, and **8p** in the AlphaScreen and reporter gene assays. Demonstrated curves are from one of the three experiments. For the Alphascreen assay, the IC_{50} values were 2.01, 3.59, 73.25, 5.88 μM; for Gal4-RORγLBD, the IC_{50} values were 0.54, 0.14, 0.04, 0.05, 0.09 μM; and for full length RORγ, the IC_{50} values were 3.5, 0.15, 0.05, 0.02, and 0.08 μM respectively.

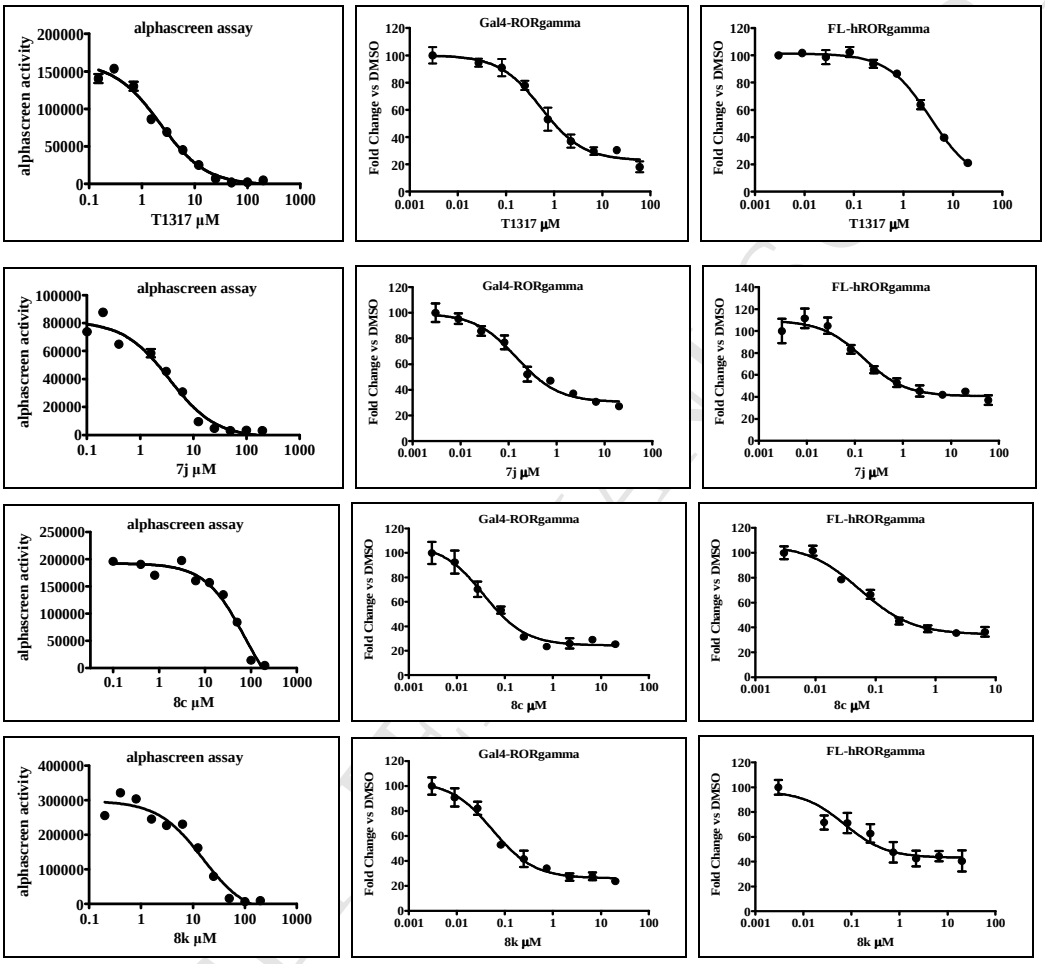

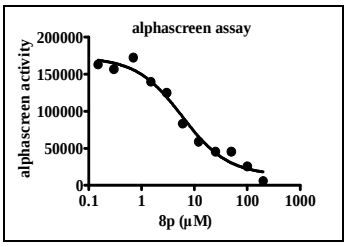

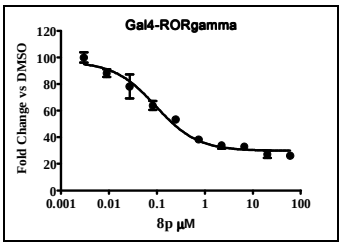

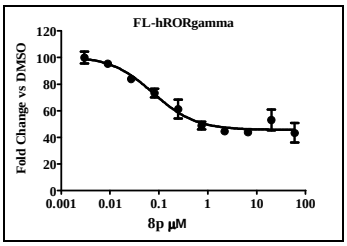

Supplementary Figure S5: ^{1}H-NMR and ^{13}C-NMR spectra of compounds **6f**, **7a**, **7k**, **8a**, **8c**, **8i**, **8k**, and **8s**.

*1-ethyl-N-(isoquinolin-7´-yl)-2-oxo-1,2-dihydrobenzo[cd]indole-6-sulfonamide(**6f**).*

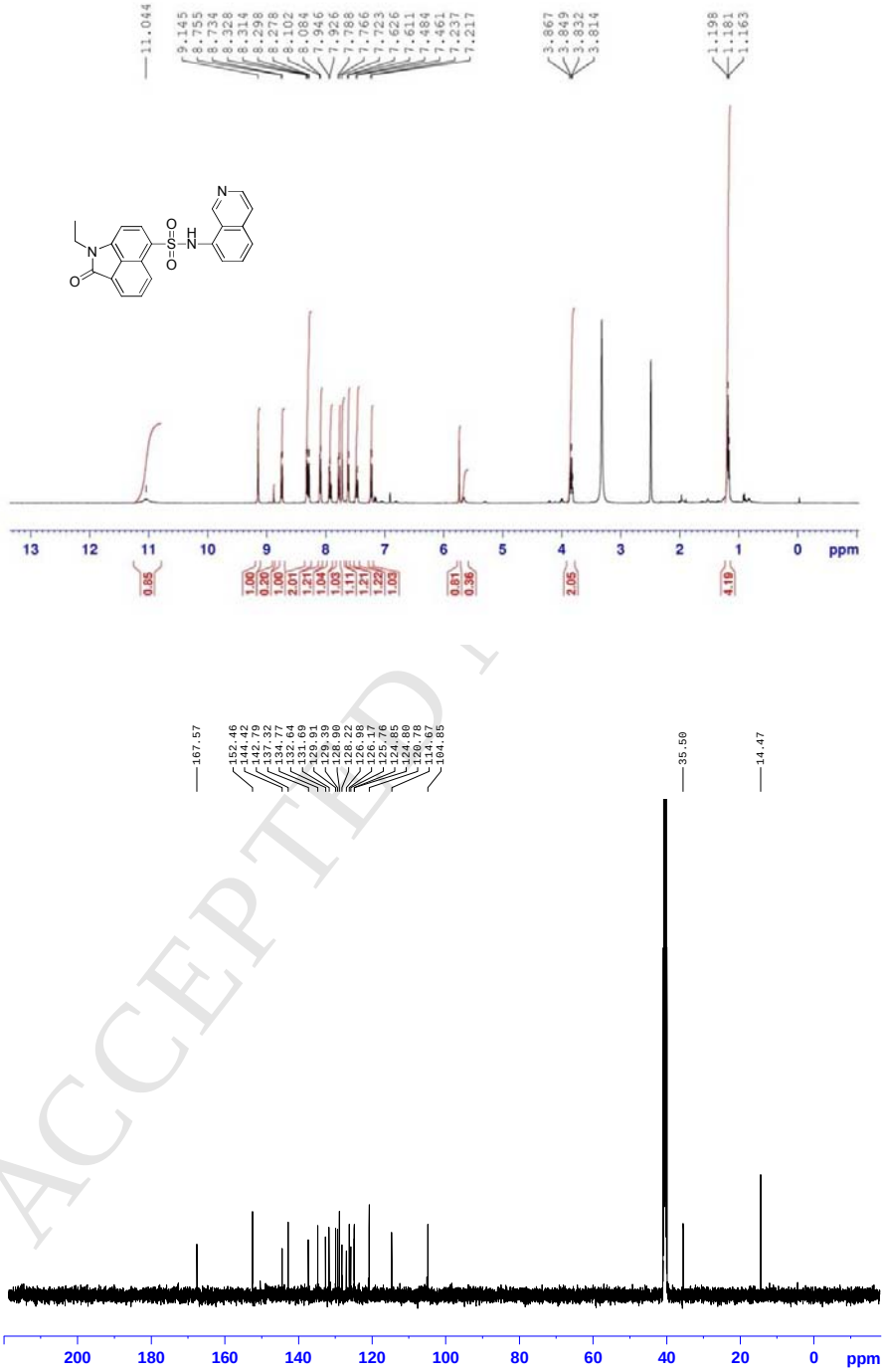

1-ethyl-N-(4´-morpholinophenyl)-2-oxo-1,2-dihydrobenzo[cd]indole-6-sulfonamide ***(7a)****.*

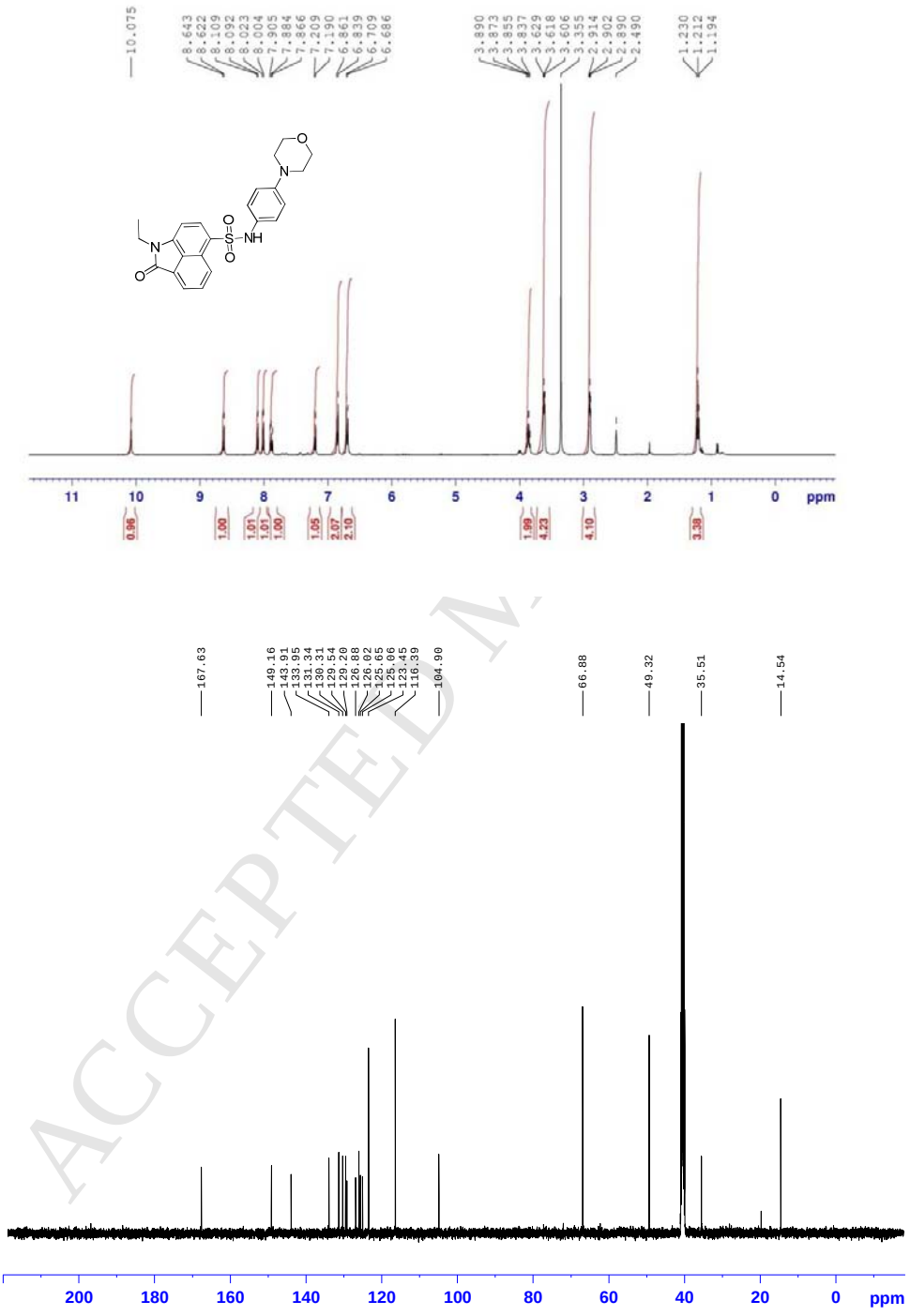

*(E)-1-ethyl-2-oxo-N-(4´-(phenyldiazenyl)phenyl)-1,2-dihydrobenzo[cd]indole-6-sulfo namide(**7k**).*

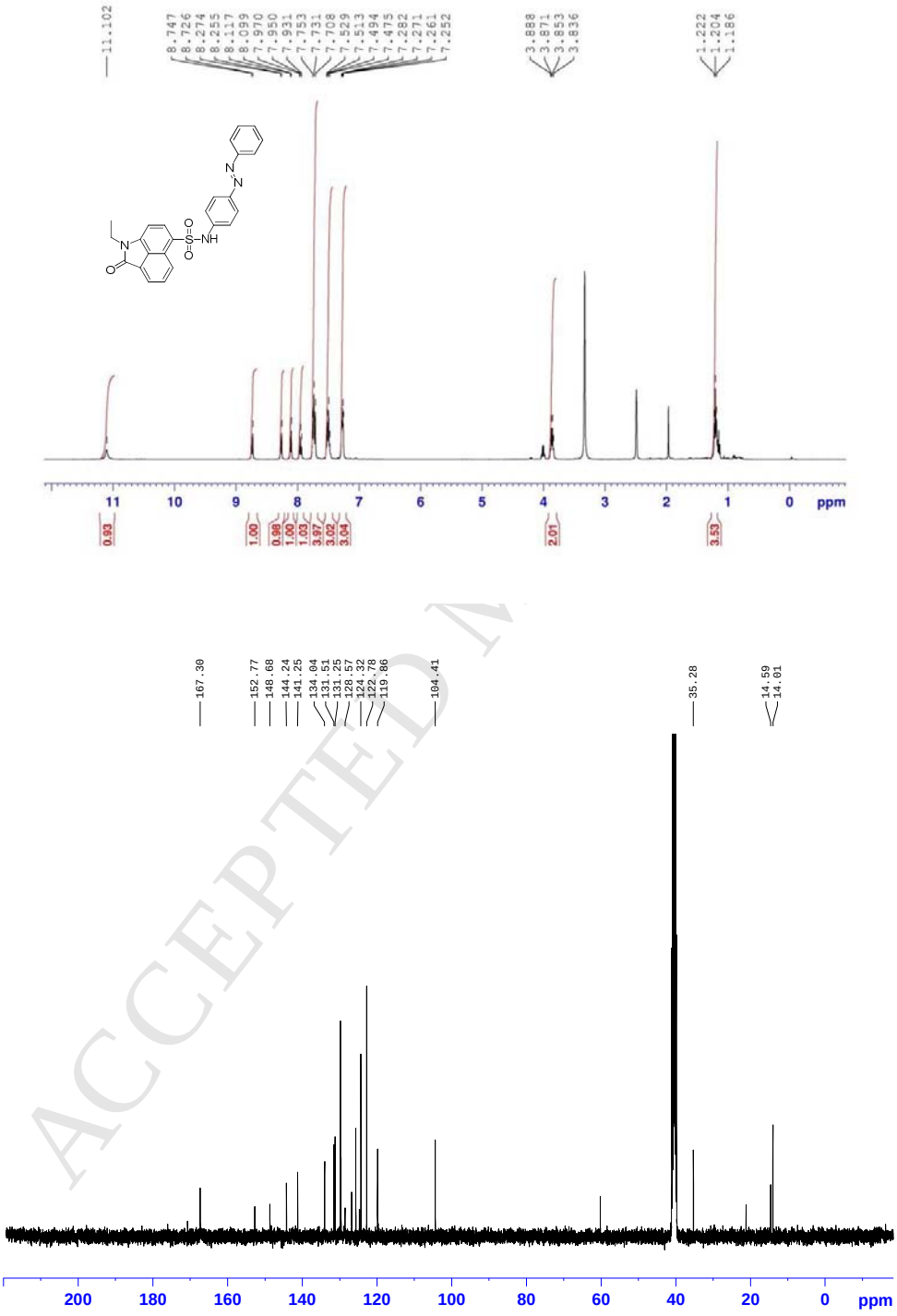

*Tert-butyl(3´-(1-ethyl-2-oxo-1,2-dihydrobenzo[cd]indole-6-sulfonamido)phenyl)carba mate(**8a**).*

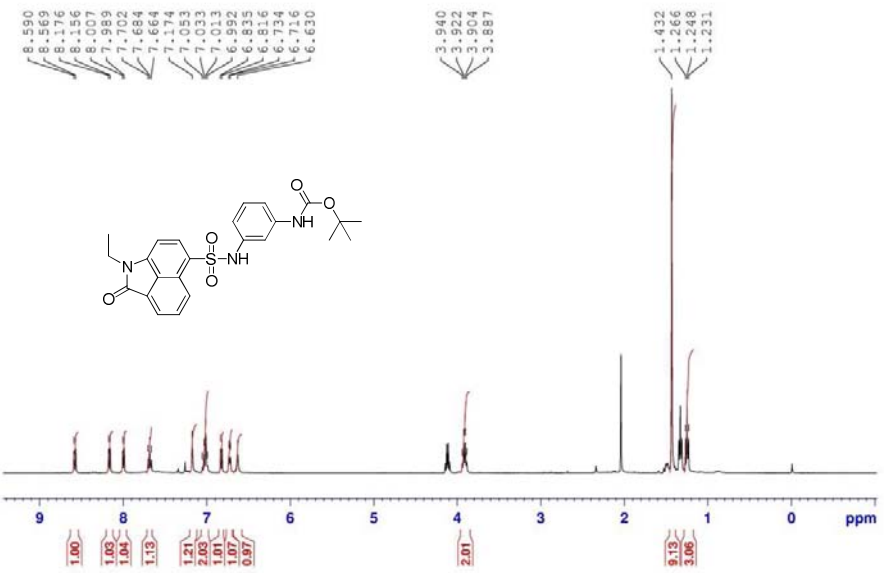

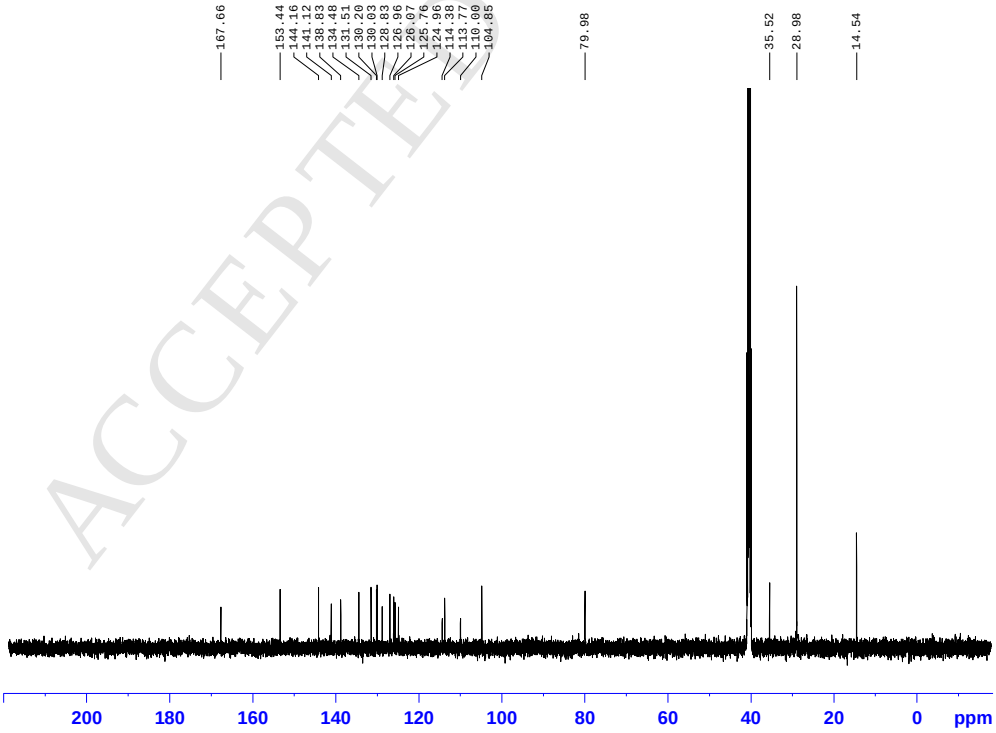

*N-(4´-acetylphenyl)-1-ethyl-2-oxo-1,2-dihydrobenzo[cd]indole-6-sulfonamide(**8c**).*

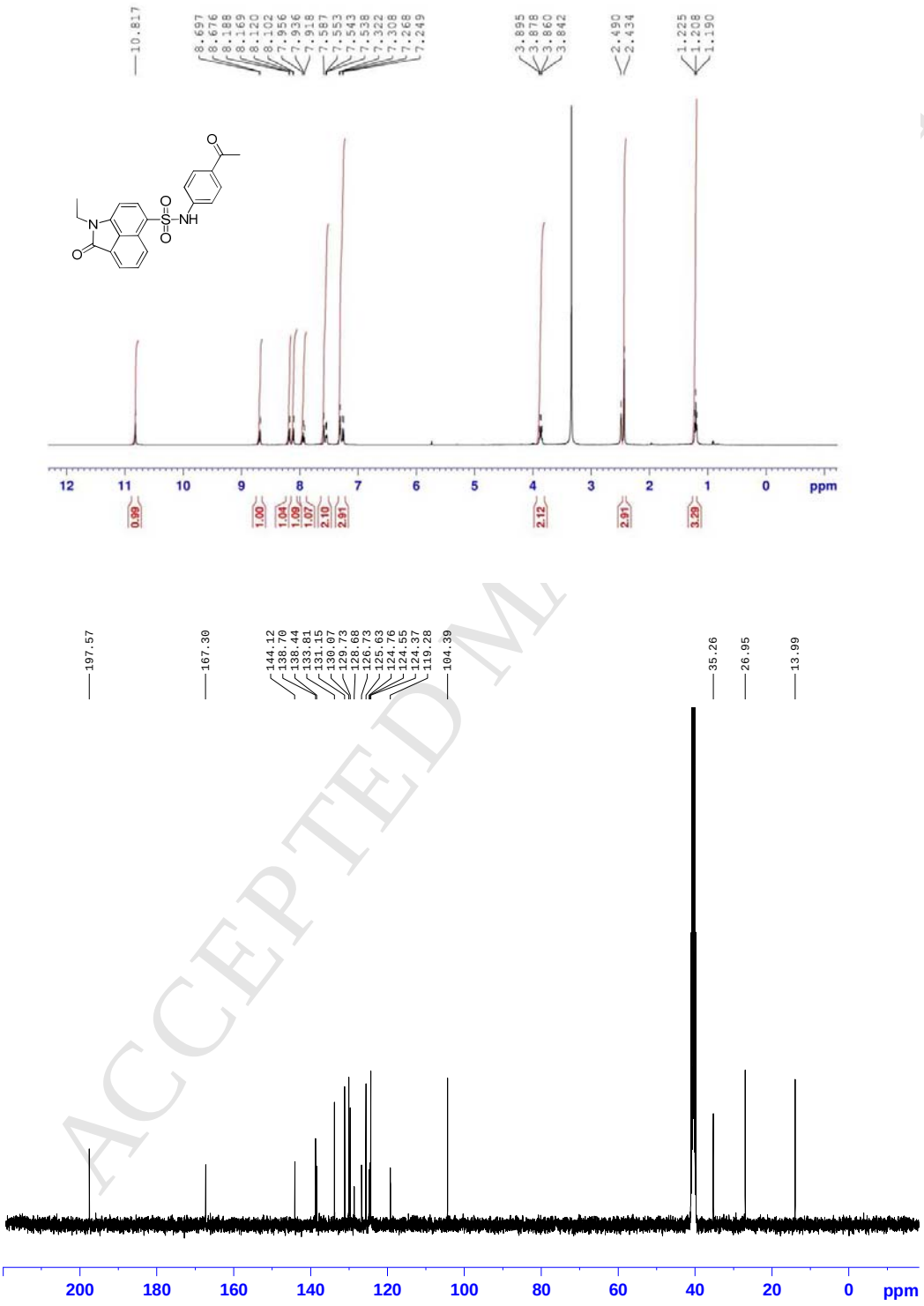

N-(2´-(tert-butyl)phenyl)-1-ethyl-2-oxo-1,2-dihydrobenzo[cd]indole-6-sulfonamide ***(8i)***.

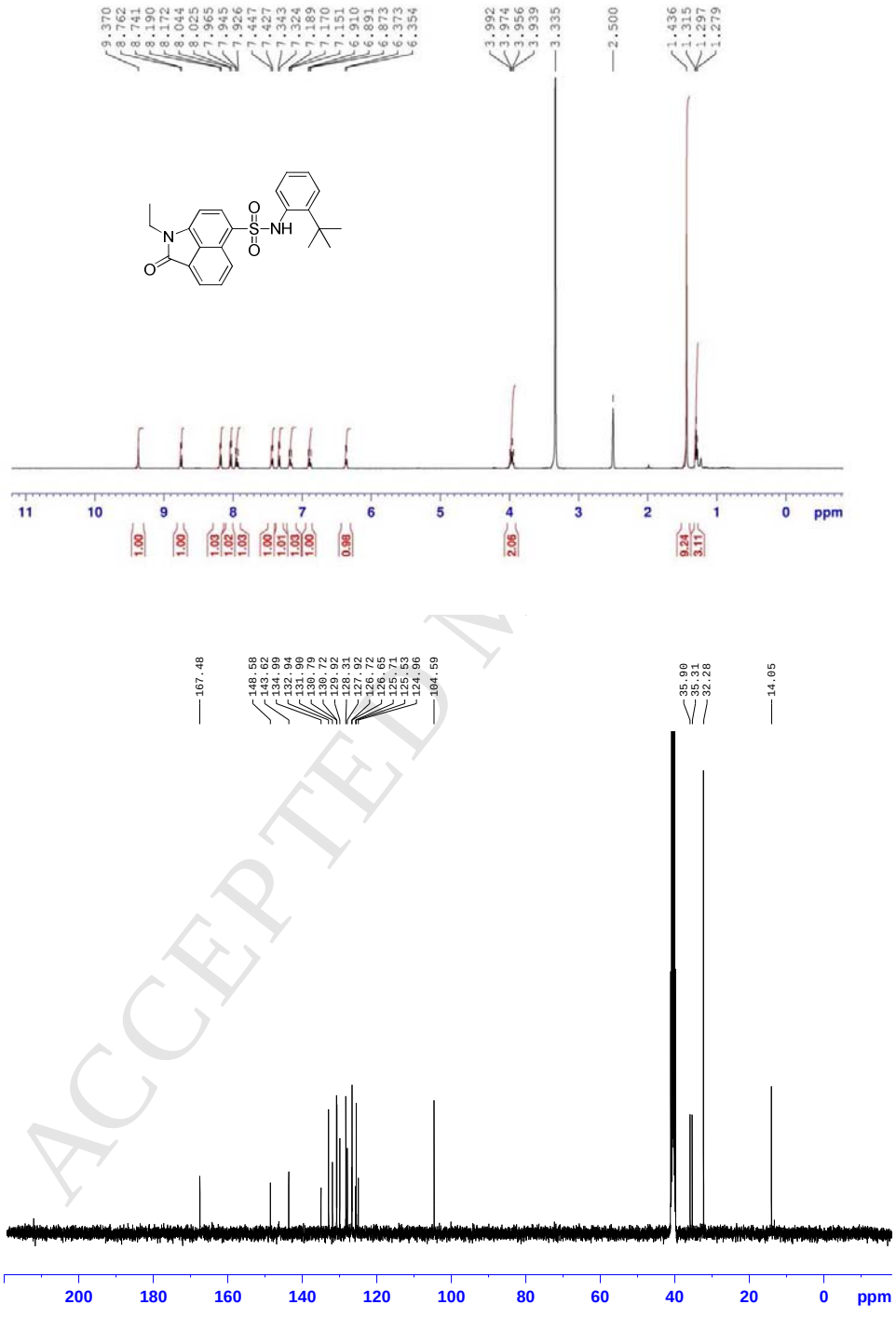

N-(3´,4´dimethoxyphenyl)-1-ethyl-2-oxo-1,2-dihydrobenzo[cd]indole-6-sulfonamide ***(8k)****.*

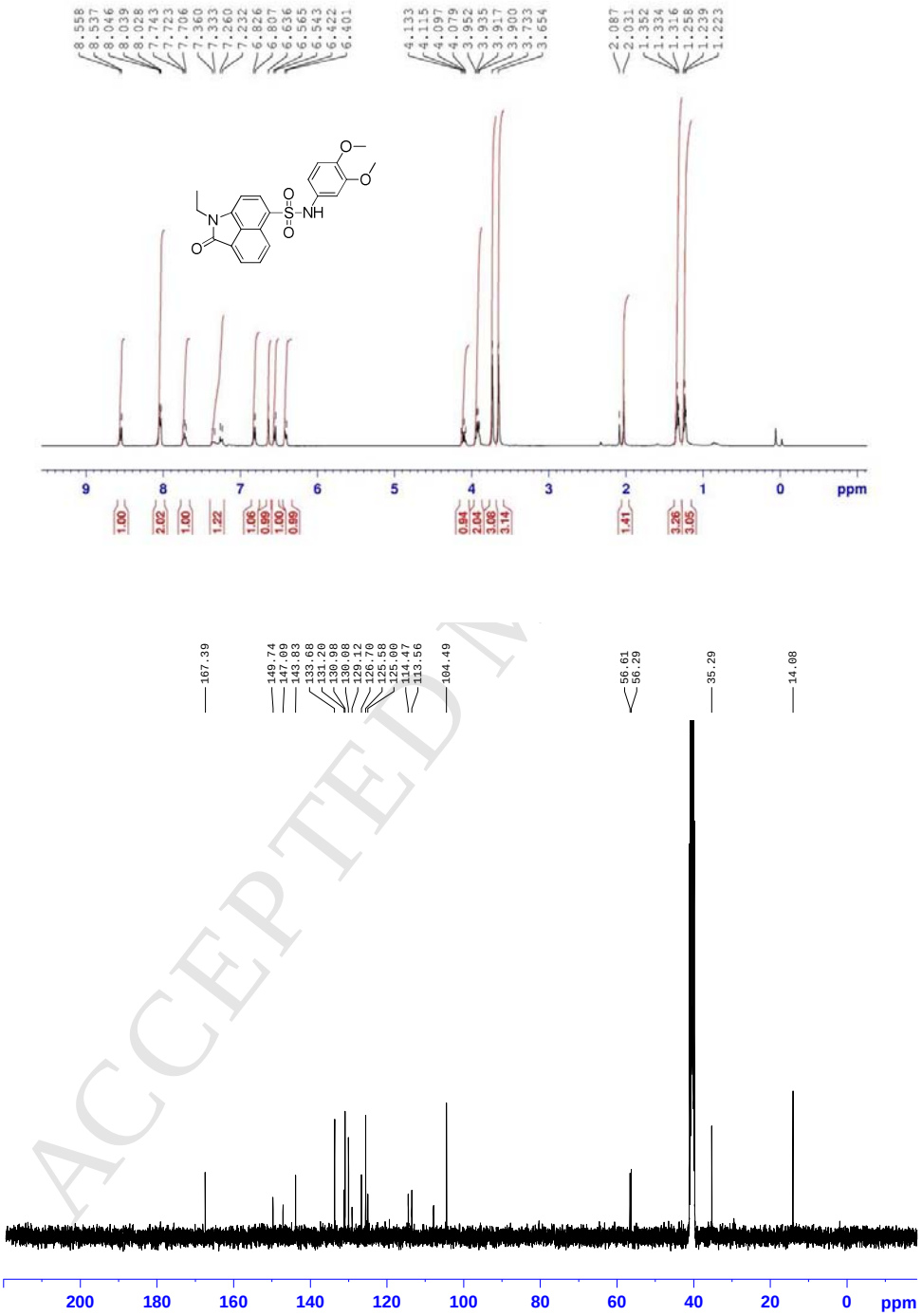

N-(2´,5´-dichlorobenzyl)-1-ethyl-2-oxo-1,2-dihydrobenzo[cd]indole-6-sulfonamide ***(8s).***